Cognitive Hierarchy in Day-to-day Network Flow Dynamics

Minyu Shen[a], Feng Xiao*[b], Weihua Gu[c], and Hongbo Ye[c]

[a]School of Management Science and Engineering, Southwestern University of Finance and Economics, China
[b]Business School, Sichuan University, China
[c]Department of Electrical and Electronic Engineering, The Hong Kong Polytechnic University

Abstract

When making route decisions, travelers may engage in a certain degree of reasoning about what the others will do in the upcoming day, rendering yesterday's shortest routes less attractive. This phenomenon was manifested in a recent virtual experiment that mimicked travelers' repeated daily trip-making process. Unfortunately, prevailing day-to-day traffic dynamical models failed to faithfully reproduce the collected flow evolution data therein. To this end, we propose a day-to-day traffic behavior modeling framework based on the Cognitive Hierarchy theory, in which travelers with different levels of strategic-reasoning capabilities form their own beliefs about lower-step travelers' capabilities when choosing their routes. Two widely-studied day-to-day models, the Network Tatonnement Process dynamic and the Logit dynamic, are extended into the framework and studied as examples. Calibration of the virtual experiment is performed using the extended Network Tatonnement Process dynamic, which fits the experimental data reasonably well. We show that the two extended dynamics have multiple equilibria, one of which is the classical user equilibrium. While analyzing global stability is intractable due to the presence of multiple equilibria, local stabilities near equilibria are developed analytically and verified by numerical experiments. General insights on how key parameters affect the stability of user equilibria are unveiled.

Keywords: day-to-day traffic dynamics; cognitive hierarchy; strategic thinking; route choice behavior; experiment calibration

*Corresponding author. Email: evan.fxiao@gmail.com

1 Introduction

Wardrop's first principle characterizes a steady-state User Equilibrium (UE) wherein no driver can reduce their travel time by unilaterally changing the route. However, due to the ever-changing nature of a transportation network (e.g., induced by traffic incidents, capacity modifications, and network structure changes), traffic states may always be in a disequilibrium state (Kumar and Peeta, 2015). To explain how travelers adjust their route-choice behaviors and predict those out-of-equilibrium states, various day-to-day traffic-network flow models have been proposed in the literature over the years.

Most day-to-day models, either continuous or discrete, focus on modeling the impact of *past* flow evolution on travelers' route choice behavior of *today*. The differences among the experienced travel times are the internal driving force that induces the flow change. For example, a rational behavior adjustment process (RBAP) proposed in Yang and Zhang (2009) generalizes a kind of flow evolution process along which the total travel cost of today will decrease based on the experienced cost of yesterday. A bunch of day-to-day models, including the proportional-switch adjustment (Smith, 1984), the projected dynamical system (Nagurney and Zhang, 1997), the network tatonnement process (Friesz et al., 1994), the evolutionary traffic dynamic (Sandholm, 2010) and the simplex gravity flow dynamic (Smith, 1983), can be categorized into this framework. Some studies also use the learning behavior (specifically an exponential smoothing filter) to model the impact of the whole historical cost trajectory on today's route choice (Horowitz, 1984; Bie and Lo, 2010; Xiao et al., 2016, 2019).

Largely ignored in the existing modeling efforts is the fact that travelers may predict what other travelers will do in the *future* (upcoming day). Substantial evidence in psychological studies demonstrates that when making decisions, people engage in a certain degree of reasoning about what others will do, i.e., a theory of mind, the ability to understand another person's mental state (Lo, 2017). In a route-choice context, suppose now a transportation network is in a disequilibrium state, and travelers in the costlier route have the incentive to switch to the shortest route with the minimum travel time. A traveler may reason like: "if many travelers choose the shortest route, then I will try to avoid being on that route". This phenomenon was somehow manifested in a recent day-to-day virtual experiment (Ye et al., 2018), but the models calibrated in that study did not take it into account. Without modeling such a logic, the prevailing day-to-day models are more like a way of calculating the final equilibrium (e.g., Hazelton

and Watling, 2004) rather than explaining the inherent reasons for traffic flow evolution. Intuitively, if all the selfish travelers have yesterday's complete information and do not consider what the others will do, the shortest one will be the only choice. Under this circumstance, the flow evolution trajectory may oscillate permanently among different routes.

To model the travelers' prediction behaviors, this paper employs the idea of Cognitive Hierarchy (CH) theory from Camerer et al. (2004), in which travelers form their beliefs of their opponents using an iterated reasoning process. In the CH theory, the heterogeneous players differ in their strategic-reasoning levels (i.e., cognitive capacities): while lower-step players do not carefully think through the whole game, the higher-step players would try to reap benefits by predicting how these lower-level "careless" players respond to the current situation. The CH model provided superior explanations in many game-theoretic settings, including guessing games (Costa-Gomes and Crawford, 2006) and extensive-form games (Ho and Su, 2013). It can also explain many phenomena in economics, marketing, and operation management, including market entry competition (Goldfarb and Xiao, 2011) and capacity allocation games (Cui and Zhang, 2017). It is worth mentioning that although the idea stemmed from Camerer et al. (2004), our proposed model's novelty lies in its dynamic nature. In contrast, most applications of the CH model in the literature are static one-shot games such as the p-beauty game.

In the literature, two pieces of work have recognized and modeled such prediction behavior; see He and Liu (2012) and He and Peeta (2016). However, they still have their limitations. The former work predicted the potential future congestion only once, and the prediction memory gradually vanished as time wore on. The latter work focused on the case where all the travelers are homogenous 1-step travelers; i.e., they all believe that the other travelers except herself are 0-step ones who myopically switch to shorter routes based on previous experience. Moreover, the model was developed using ordinary differential equations. Despite their tractability for mathematical analysis, the continuous models bring challenges in calibration with real data because the real-world system of repeated daily trips is discrete. Some properties (e.g., stability) in continuous time can only be considered a weaker result compared to the discrete-time counterpart (Li et al., 2018). Under some scenarios, conclusions drawn from continuous- and discrete-time systems may even contradict each other (Ye et al., 2021).

In this paper, we establish a general framework of day-to-day network flow dynamics based on the CH theory to analyze travelers' dynamic routing behaviors. In this framework, we allow the travelers to be heterogeneous in their strategic-reasoning capabilities and to form their

own beliefs about other travelers' strategic-reasoning capabilities and actions. We extend two widely-studied dynamics in the literature, the network tatonnement process (NTP) dynamic (for deterministic UE, DUE) and the Logit dynamic (for stochastic UE, SUE), into our CH framework and call them CH-NTP and CH-Logit dynamic, respectively. A previous online virtual experiment in Ye et al. (2018), which conventional day-to-day models could not fit, can now be calibrated by our proposed CH-NTP dynamic reasonably well. Moreover, the models predict that strategic-reasoning behaviors would lead the system to multiple equilibria, one of which being the classical user equilibrium. Jacobian matrices at the equilibrium points are derived and used to form analytical criteria on local stability around a user equilibrium. Theoretical results and numerical experiments unveiled several insights into how key parameters affect the local stability.

The rest of the paper is organized as follows. The following section describes the general modeling framework. The CH-NTP dynamic is presented in Section 3 as the DUE example of the framework. Calibration of the real-world experiment with CH-NTP dynamic is furnished in Section 4. Section 5 provides numerical experiments regarding the CH-NTP dynamic. As the SUE example, the CH-Logit dynamic is presented in Section 6. Conclusions are drawn in Section 7 with discussions on future research directions.

2 Modeling Framework

2.1 Setups

We consider a strongly-connected transportation network $G(N, L, W)$ consisting of a set N of nodes, a set L of links, and a set W of origin–destination (OD) pairs. Each OD pair, $w \in W$, has a travel demand of d_w and is connected by a set R_w of routes. Travelers in the network are categorized into a set K (with $|K|$ denoting the cardinality) of classes (steps) by their cognitive-capacity levels. (Throughout this paper, the terms "class" and "step" are used interchangeably.) We assume for simplicity that the proportion of k-step travelers, p^k ($k \in K$ and $\sum_{k=0}^{|K|-1} p^k = 1$), is the same across all the OD pairs. This assumption allows us to write the scaled feasible route flow set of k-step travelers as $\Omega_{p^k} \equiv \{\boldsymbol{x}^k | \Gamma \boldsymbol{x}^k = p^k \boldsymbol{d}, \boldsymbol{x}^k \geq 0\}$, where $\boldsymbol{x}^k \equiv (x^k_{rw}, r \in R_w, w \in W)^T$ is the route flow vector (pattern) of class $k \in K$, $\boldsymbol{d} \equiv (d_w, w \in W)^T$ is the OD demand vector and Γ is an OD-route incidence matrix indicating if a route belongs to an OD pair. The superscript "T" represents the transpose operation. With a little abuse of notation, we denote Ω_η as the feasible

route flow set with *scaled* OD demand $\eta \boldsymbol{d}, \eta \in (0, 1]$. Denote $c_{rw}(\boldsymbol{x})$ as the actual travel time of route $r \in R_w, w \in W$, under any route flow pattern $\boldsymbol{x} \in \Omega_1$, and $\boldsymbol{c}(\boldsymbol{x}) \equiv (c_{rw}(\boldsymbol{x}), r \in R_w, w \in W)^T$. Assume that $\boldsymbol{c}(\boldsymbol{x})$ is continuous in $\boldsymbol{x}$.

2.2 Flow update rules

On day t, the route flow pattern of k-step is denoted as $\boldsymbol{x}^{k,(t)}$, and the aggregate observed route flow pattern $\tilde{\boldsymbol{x}}^{(t)} = \sum_k \boldsymbol{x}^{k,(t)}$. By observing $\tilde{\boldsymbol{x}}^{(t)}$ (or receiving it from the advanced traveler information system), a k-step traveler before trip will predict the route flow pattern on $(t+1)$-th day as per her cognitive capacity level (see subsequent Section 2.3). The predicted route flow pattern and its corresponding travel cost pattern are denoted as $\boldsymbol{\pi}^{k,(t+1)}$ and $\boldsymbol{c}\left(\boldsymbol{\pi}^{k,(t+1)}\right)$, respectively. With $\boldsymbol{x}^{k,(t)}$ and $\boldsymbol{c}\left(\boldsymbol{\pi}^{k,(t+1)}\right)$, the flow pattern of k-step travelers on the next day $t+1$ can be updated as:

$$\boldsymbol{x}^{k,(t+1)} = H_{\Omega_{p^k}}\left[\boldsymbol{x}^{k,(t)}, \boldsymbol{c}\left(\boldsymbol{\pi}^{k,(t+1)}\right); \alpha, \zeta\right] \equiv \alpha \boldsymbol{y}\left[\boldsymbol{x}^{k,(t)}, \boldsymbol{c}\left(\boldsymbol{\pi}^{k,(t+1)}\right); \zeta\right] + (1-\alpha)\boldsymbol{x}^{k,(t)}, \tag{1}$$

where $\boldsymbol{y}$ is the "target" flow pattern in Ω_{p^k} determined by a specific day-to-day dynamical model parameterized by ζ; and the exponential-moving-average coefficient, $\alpha \in (0, 1)$, reflecting travelers' inertia or reluctance to change. (The larger the α, the smaller the inertia.) Note that the predicted flow pattern for any k, $\boldsymbol{\pi}^{k,(t+1)}$, is always in Ω_1.

Our model does not incorporate memory and learning processes in travelers' decision-making. If we were to include memory effects, travelers' route choices might be influenced by a weighted average of past experiences rather than just the most recent one (Horowitz, 1984; Bie and Lo, 2010; Xiao et al., 2016; Ye et al., 2021). By abstracting away memory and learning, we can more clearly isolate and analyze the impacts of travelers' strategic thinking behavior on network dynamics. This simplification allows for greater analytical tractability and easier interpretation of results.

By describing the dynamic in such a general way, most day-to-day models in the literature can be applied to the framework. For example, the day-to-day models satisfying the RBAP property (Yang and Zhang, 2009) can be applied, i.e., any $\boldsymbol{y}[\cdot]$ satisfying:

$$\boldsymbol{y}\left[\boldsymbol{x}^{k,(t)}, \boldsymbol{c}\left(\boldsymbol{\pi}^{k,(t+1)}\right); \zeta\right] \begin{cases} \in \Psi^{k,(t)}, \Psi^{k,(t)} \neq \\ = \boldsymbol{x}^{k,(t)}, \Psi^{k,(t)} = \end{cases}, \tag{2}$$

where $\Psi^{k,(t)} \equiv \left\{ \boldsymbol{y} | \boldsymbol{y} \in \Omega_{p^k}, \boldsymbol{y}^T \boldsymbol{c}\left(\boldsymbol{\pi}^{k,(t+1)}\right) < (\boldsymbol{x}^{k,(t)})^T \boldsymbol{c}\left(\boldsymbol{\pi}^{k,(t+1)}\right) \right\}$ is the feasible route flow set of k-step for which the k-step travelers' total travel costs based on the *predicted* costs decreases.

Moreover, applications of the framework are not confined to deterministic day-to-day models; i.e., the $\boldsymbol{y}[\cdot]$ can also be in a stochastic sense. For example, Logit-based stochastic day-to-day models contained in the "SUE version" of the RBAP framework (Xiao et al., 2019) can be adopted. In this paper, we study two typical examples for the DUE and SUE, respectively.

2.3 Cognitive hierarchy levels

We now use the CH theory to model how travelers with different cognitive capacities form their beliefs on the next day's flow pattern. To start, 0-step travelers do not think strategically at all. They deem that the flow pattern of day t will remain unchanged on day $t+1$:

$$\boldsymbol{\pi}^{0,(t+1)} = \tilde{\boldsymbol{x}}^{(t)}. \tag{3}$$

It is clear that if the network only contains the 0-step travelers, it degenerates into a conventional day-to-day model. (In a CH model for the one-shot games, 0-step players were assumed to either randomize equally across all strategies or choose a salient strategy using *ex-ante* information (Camerer et al., 2004). Here we adopt the latter idea.)

As per the CH theory (Camerer et al., 2004), the $k(k \geq 1)$-step travelers try to take advantage by predicting how lower-step players respond to the current flow pattern, but are *overconfident* and do not realize others are using exactly as many thinking steps as they are. Denote $q_k^h = \frac{p^h}{\sum_{i=0}^{k-1} p^i}$ as k-step travelers' belief about the normalized proportion of h-step travelers and $q_k^h = 0$ for $\forall h \geq k$. As consistent with the CH theory, such a setting means that travelers do not know the exact distribution of lower-step travelers — they only confidently assume the normalized distribution. (This setting was also adopted in other studies; see, e.g., Cui and Zhang (2017) that apply the CH theory to the capacity allocation games in the operation management field.)

Based on the above idea, a 1-step traveler thinks that all the others are 0-step travelers, i.e., $q_1^0 = \frac{p^0}{p^0} = 1$. Her predicted flow on day $t+1$ is thus formed by looking one step ahead:

$$\boldsymbol{\pi}^{1,(t+1)} = H_{\Omega_{q_1^0}}\left[q_1^0 \tilde{\boldsymbol{x}}^{(t)}, \boldsymbol{c}\left(\boldsymbol{\pi}^{0,(t+1)}\right); \hat{\alpha}, \hat{\zeta}\right] = H_{\Omega_1}\left[\tilde{\boldsymbol{x}}^{(t)}, \boldsymbol{c}\left(\tilde{\boldsymbol{x}}^{(t)}\right); \hat{\alpha}, \hat{\zeta}\right], \tag{4}$$

where $\hat{\alpha} \in (0,1)$ and $\hat{\zeta}$ are the predicted coefficients in the travelers' minds.

With this predicted flow pattern, the 1-step travelers will switch the route choice, and the resultant flow pattern becomes:

$$\boldsymbol{x}^{1,(t+1)} = H_{\Omega_{p^1}}\left[\boldsymbol{x}^{1,(t)}, \boldsymbol{c}\left(\boldsymbol{\pi}^{1,(t+1)}\right); \alpha, \zeta\right] = H_{\Omega_{p^1}}\left[\boldsymbol{x}^{1,(t)}, \boldsymbol{c}\left(H_{\Omega_1}\left[\tilde{\boldsymbol{x}}^{(t)}, \boldsymbol{c}\left(\tilde{\boldsymbol{x}}^{(t)}\right); \hat{\alpha}, \hat{\zeta}\right]\right); \alpha, \zeta\right]. \quad (5)$$

2-step travelers will jointly predict both 0-step and 1-step travelers' responses. The normalized proportion of these two types are $q_2^0 = \frac{p^0}{p^0+p^1}$ and $q_2^1 = \frac{p^1}{p^0+p^1}$, respectively. They anticipate that the flow pattern of the next day will be:

$$\boldsymbol{\pi}^{2,(t+1)} = H_{\Omega_{q_2^0}}\left[q_2^0\tilde{\boldsymbol{x}}^{(t)}, \boldsymbol{c}\left(\boldsymbol{\pi}^{0,(t+1)}\right); \hat{\alpha}, \hat{\zeta}\right] + H_{\Omega_{q_2^1}}\left[q_2^1\tilde{\boldsymbol{x}}^{(t)}, \boldsymbol{c}\left(\boldsymbol{\pi}^{1,(t+1)}\right); \hat{\alpha}, \hat{\zeta}\right]. \quad (6)$$

Here we assume that the travelers of k-step ($k \geq 1$) share the same predicted parameters, $\hat{\alpha}$, and $\hat{\zeta}$. This assumption allows us to *qualitatively* model whether the higher-step travelers over- or under-predict lower-step travelers' behaviors. It also keeps our model parsimonious. Despite this simple treatment, as we will see in the subsequent Section 4, the model still captures the virtual-experiment data quite well, even when we further set $\hat{\alpha} = \alpha$ and $\hat{\zeta} = \zeta$!

Based on the predicted flow pattern $\boldsymbol{\pi}^{2,(t+1)}$, the 2-step travelers update their route choices as follows:

$$\begin{aligned}\boldsymbol{x}^{2,(t+1)} &= H_{\Omega_{p^2}}\left[\boldsymbol{x}^{2,(t)}, \boldsymbol{c}\left(\boldsymbol{\pi}^{2,(t+1)}\right); \alpha, \zeta\right] \\ &= H_{\Omega_{p^2}}\left[\boldsymbol{x}^{2,(t)}, \boldsymbol{c}\left(H_{\Omega_{q_2^0}}\left[q_2^0\tilde{\boldsymbol{x}}^{(t)}, \boldsymbol{c}\left(\boldsymbol{\pi}^{0,(t+1)}\right); \hat{\alpha}, \hat{\zeta}\right] + H_{\Omega_{q_2^1}}\left[q_2^1\tilde{\boldsymbol{x}}^{(t)}, \boldsymbol{c}\left(\boldsymbol{\pi}^{1,(t+1)}\right); \hat{\alpha}, \hat{\zeta}\right]\right); \alpha, \zeta\right].\end{aligned} \quad (7)$$

The rest types of travelers ($k > 2$) can be done in a recursive manner as follows:

$$\begin{cases}\boldsymbol{\pi}^{k,(t+1)} = \sum\limits_{0\leq h<k} H_{\Omega_{q_k^h}}\left[q_k^h\tilde{\boldsymbol{x}}^{(t)}, \boldsymbol{c}\left(\boldsymbol{\pi}^{h,(t+1)}\right)\right]; \hat{\alpha}, \hat{\zeta}]; \\ \boldsymbol{x}^{k,(t+1)} = H_{\Omega_{p^k}}\left[\boldsymbol{x}^{k,(t)}, \boldsymbol{c}\left(\boldsymbol{\pi}^{k,(t+1)}\right); \alpha, \zeta\right].\end{cases} \quad (8)$$

Substantial experiments in the behavioral game theory found that the average thinking step across all the players lies between 1 and 2 (Camerer et al., 2004; Chong et al., 2016). Hence, the rest of this paper focuses on the case where $|K| \leq 3$. Note that those experiments were designed for one-shot games with a relatively small number of subjects, in contrast to the dynamic setting with many subjects in this paper. It is also worth mentioning that the methodology in this paper can also be applied to cases where $|K| > 3$.

2.4 Model interpretation and practical relevance

2.4.1 Interpretations on the strategic thinking

Strategic thinking behavior is the core component of our proposed modeling framework. As stemmed from the CH theory (Camerer et al., 2004), our model assumes travelers know other travelers' strategic levels (represented by q_k^h). This assumption may seem unrealistic at first glance since individual travelers are unlikely to have explicit information about the distribution of strategic sophistication among other road users. However, it can be interpreted on several grounds:

1. Assuming knowing lower-step travelers' strategic levels serves as a simplified heuristic that represents the underlying cognitive processes travelers use to anticipate others' behavior. While individual travelers may not explicitly possess this information, our model captures the essence of strategic thinking *in aggregate*. This approach is validated by the model's improved fit to observed data (see Section 4), suggesting it effectively captures important aspects of real-world strategic behavior in transportation networks. Notably, even the 1-step model ($|K| = 2$) provides considerable improvements while requiring only one additional parameter compared to traditional day-to-day models. The fact that a multi-class day-to-day model with additional parameters but without strategic prediction failed to reproduce the experimental data further supports that our model's success stems from its ability to capture strategic thinking, not merely from increased parameter flexibility.

2. The q_k^h values might be interpreted as aggregate *beliefs* held by a class of travelers, rather than exact knowledge possessed by individuals. This aggregate approach allows us to model the overall effect of strategic thinking without making strong claims about individual cognition. The aggregate beliefs represented by q_k^h can be seen as emergent properties of the system, arising from the collective experience of travelers over time, rather than explicit individual knowledge.

3. Our modeling framework aligns with the "theory of mind" concept from cognitive psychology - the ability to attribute mental states and intentions to others (Lo, 2017). In our transportation context, the strategic levels and associated beliefs represent simplified versions of travelers' theory of mind about other road users.

2.4.2 Practical relevance

Our modeling framework may be used to characterize the strategic thinking behaviors of major decision-making entities that each control a significant portion of traffic flow. In this context, the flow distribution vector of one class can be viewed as a decision of one large entity. This approach is particularly relevant in modern urban environments where traffic patterns are increasingly influenced by sophisticated navigation systems and centralized management centers. These systems operate at different levels of sophistication in predicting and responding to traffic conditions. At the most basic level ($k = 0$), we have navigation systems or drivers simply reacting to current traffic conditions without strategic planning. The next level ($k = 1$) includes more advanced navigation platforms like Google Maps and Waze, which not only provide route recommendations based on current conditions but also engage in predictive behavior (Lau, 2020). By anticipating the actions of other road users and potential congestion points, they aim to recommend shorter routes for their users, effectively playing a strategic game against other decision-makers in the network. At higher level of sophistication ($k = 2$ or above) are advanced traffic management centers and mobility service providers. These entities attempt to optimize overall traffic flow by considering multiple levels of interaction between different road user groups. Their decisions may require anticipating the responses of various traveler segments and adjusting traffic control measures accordingly.

3 CH-NTP Dynamic

The previous section describes the idea using a general day-to-day operator $H[\cdot]$. This section specifies $H[\cdot]$ as the particular NTP dynamic that admits DUE as a fixed point and analyzes its mathematical properties. The NTP dynamic's behavioral explanation is identical to a link-based day-to-day model proposed in He et al. (2010): travelers seek to minimize their travel costs while exerting some efforts (or incurring costs) to deviate from incumbent routes. This explanation was also discovered by Tsakas and Voorneveld (2009) in the game theory literature in which the NTP dynamic was called the target projection dynamic. In addition, the NTP dynamic has a unified closed-form formula with the projected dynamical system when route flows only evolve in the interior of the feasible route flow set (Nagurney and Zhang, 1997; Guo et al., 2015; Xiao et al., 2016).

In a discrete version, for every k-step traveler, the CH-NTP dynamic reads

$$\boldsymbol{x}^{k,(t+1)} - \boldsymbol{x}^{k,(t)} = \alpha\left(P_{\Omega_{p^k}}\left[\boldsymbol{x}^{k,(t)} - \gamma \boldsymbol{c}\left(\boldsymbol{\pi}^{k,(t+1)}\right)\right] - \boldsymbol{x}^{k,(t)}\right), k \in K, \tag{9}$$

where $P_{\Omega_\eta}[\boldsymbol{z}]$ is the projection operator that solves the optimization $\arg\min_{\boldsymbol{h}\in\Omega_\eta}\|\boldsymbol{h}-\boldsymbol{z}\|^2$. The ζ in (1) is now replaced by $\gamma(>0)$, which captures the costs incurred by deviations from the incumbent routes. With a larger γ, travelers have smaller inertia and are prone to switching.

Based on the modeling framework in Section 2.3, the predicted flow pattern of each class $k \in \{0,1,2\}$ is given by:

$$\boldsymbol{\pi}^{0,(t+1)} = \tilde{\boldsymbol{x}}^{(t)}, \tag{10}$$

$$\boldsymbol{\pi}^{1,(t+1)} = \hat{\alpha} P_{\Omega_1}\left[\tilde{\boldsymbol{x}}^{(t)} - \hat{\gamma}\boldsymbol{c}\left(\boldsymbol{\pi}^{0,(t+1)}\right)\right] + (1-\hat{\alpha})\tilde{\boldsymbol{x}}^{(t)}, \tag{11}$$

$$\boldsymbol{\pi}^{2,(t+1)} = \hat{\alpha} P_{\Omega_{q_2^0}}\left[q_2^0\tilde{\boldsymbol{x}}^{(t)} - \hat{\gamma}\boldsymbol{c}\left(\boldsymbol{\pi}^{0,(t+1)}\right)\right] + \hat{\alpha} P_{\Omega_{q_2^1}}\left[q_2^1\tilde{\boldsymbol{x}}^{(t)} - \hat{\gamma}\boldsymbol{c}\left(\boldsymbol{\pi}^{1,(t+1)}\right)\right] + (1-\hat{\alpha})\tilde{\boldsymbol{x}}^{(t)}, \tag{12}$$

where the predicted parameter $\hat{\zeta}$ in (4) and (6) is replaced by $\hat{\gamma} > 0$. Eqs. (10)-(12) indicate that for each k, $\boldsymbol{\pi}^{k,(t+1)}$ is a function of $\tilde{\boldsymbol{x}}^{(t)}$.

The following lemma introduces a fundamental property of the projection operator, which will be useful in the following analyses.

Lemma 1. *(Facchinei and Pang, 2007). Let C be a nonempty and closed convex subset of $\mathcal{R}^n$. Then for any $\boldsymbol{z} \in \mathcal{R}^n$ and $\boldsymbol{w} \in C$,*

$$(P_C[\boldsymbol{z}] - \boldsymbol{z})^T(\boldsymbol{w} - P_C[\boldsymbol{z}]) \geq 0. \tag{13}$$

Moreover, $P_C[\boldsymbol{z}]$ is the only point in C satisfying the above relation.

3.1 Mixed prediction-based equilibria

Fixed points of the dynamical system (9)-(12) are termed as mixed prediction-based equilibria (MPE) and they are characterized in the following proposition.

Proposition 1. *When the route cost function $\boldsymbol{c}(\boldsymbol{x})$ is continuous, the dynamical system* (9)-(12) *admits at least one MPE (i.e., one fixed point). Moreover, a vector $\boldsymbol{x}^\diamond \equiv (\boldsymbol{x}^{k,\diamond}, \boldsymbol{x}^{k,\diamond} \in \Omega_{p^k}, k = 0,1,2)^T$ is an MPE if and only if the following variational inequality (VI) holds:*

$$\sum_{k=0,1,2} \boldsymbol{c}\left(\boldsymbol{\pi}^{k,\diamond}(\tilde{\boldsymbol{x}}^\diamond)\right)^T\left(\boldsymbol{x}^k - \boldsymbol{x}^{k,\diamond}\right) \geq 0, \forall \boldsymbol{x} \equiv (\boldsymbol{x}^0, \boldsymbol{x}^1, \boldsymbol{x}^2)^T \in \prod_{k=0,1,2}\Omega_{p^k}, \tag{14}$$

where $\boldsymbol{\pi}^{k,\Diamond}$ is a function of the aggregate flow pattern $\tilde{\boldsymbol{x}}^{\Diamond} = \sum_k \boldsymbol{x}^{k,\Diamond}$, given by (10)-(12).

Proof. Continuity of the RHS of the dynamical system (9)-(12) is guaranteed by the continuities of the projection operator (Penot, 2005) and the route cost function. Hence, according to Brouwer's Fixed Point Theorem, there exist at least one fixed point to the dynamical system.

According to Lemma 1, any fixed point of dynamical system (9)-(12), denoted as $\boldsymbol{x}^{\Diamond} \equiv (\boldsymbol{x}^{k,\Diamond}, \boldsymbol{x}^{k,\Diamond} \in \Omega_{p^k}, k = 0, 1, 2)^T$, solves the following inequalities:

$$\boldsymbol{x}^{k,\Diamond} = P_{\Omega_{p^k}}\left[\boldsymbol{x}^{k,\Diamond} - \gamma \boldsymbol{c}\left(\boldsymbol{\pi}^{k,\Diamond}(\tilde{\boldsymbol{x}}^{\Diamond})\right)\right] \Leftrightarrow \gamma \boldsymbol{c}\left(\boldsymbol{\pi}^{k,\Diamond}(\tilde{\boldsymbol{x}}^{\Diamond})\right)^T \left(\boldsymbol{x}^k - \boldsymbol{x}^{k,\Diamond}\right) \geq 0, \forall \boldsymbol{x}^k \in \Omega_{p^k}, \forall k, \tag{15}$$

where $\boldsymbol{\pi}^{k,\Diamond}$ is the predicted flow pattern under $\tilde{\boldsymbol{x}}^{\Diamond} = \sum_k \boldsymbol{x}^{k,\Diamond}$, given by (10)-(12). The right part of (15) is of a VI form and they can be combined since $\Omega_{p^k}(k \in K)$ are disjoint from each other (Kinderlehrer and Stampacchia, 2000; Yang et al., 2007) . □

We next define a $|K|$-class DUE in Definition 1 (see also in Nagurney, 2000, and Zhou et al., 2020) and show that it is one of the MPE in Proposition 2.

Definition 1. *(Nagurney, 2000; Zhou et al., 2020) A route flow pattern $\boldsymbol{x}^* \equiv (\boldsymbol{x}^{k,*}, \boldsymbol{x}^{k,*} \in \Omega_{p^k}, k \in K)^T$ is said to be a $|K|$-class DUE if the following VI holds:*

$$\sum_{k \in K} \boldsymbol{c}^k(\tilde{\boldsymbol{x}}^*)^T \left(\boldsymbol{x}^k - \boldsymbol{x}^{k,*}\right) \geq 0, \forall \boldsymbol{x} \equiv (\boldsymbol{x}^k, k \in K)^T \in \prod_{k \in K} \Omega_{p^k}, \tag{16}$$

where $\tilde{\boldsymbol{x}}^* = \sum_k \boldsymbol{x}^{k,*}$ and $\boldsymbol{c}^k(\tilde{\boldsymbol{x}}^*)$ is the experienced route cost vector of class k.

Note that the aggregate flow $\tilde{\boldsymbol{x}}^*$ equals the classical DUE of a single class in the normal sense. The superscript k can also be dropped from $\boldsymbol{c}^k(\tilde{\boldsymbol{x}}^*)$ because all the travelers have the same experience on each route. In the remainder of the paper, the prefix "$|K|$-class" will be omitted if the context allows.

Proposition 2. *A $|K|(= 3)$-class DUE in Definition 1 is an MPE of the dynamical system* (9)-(12)*, but not vice versa.*

Proof. We prove the sufficiency, and the necessity can be easily negated by a counter-example, as demonstrated in the numerical experiments (see Section 5.1).

At the DUE, first note from (10) that $\boldsymbol{\pi}^{0,*}$ equals the aggregate flow pattern, $\tilde{\boldsymbol{x}}^*$. It is well-known that $\tilde{\boldsymbol{x}}^* \in \Omega_1$ of the classical single-class DUE satisfies the following VI:

$$\boldsymbol{c}(\tilde{\boldsymbol{x}}^*)^T(\boldsymbol{x} - \tilde{\boldsymbol{x}}^*) \geq 0, \forall \boldsymbol{x} \in \Omega_1. \tag{17}$$

Multiplying (17) by $-\hat{\gamma}$ and adding $(\tilde{\boldsymbol{x}}^*)^T(\boldsymbol{x} - \tilde{\boldsymbol{x}}^*)$ to both sides yields:

$$(\tilde{\boldsymbol{x}}^* - (\tilde{\boldsymbol{x}}^* - \hat{\gamma}\boldsymbol{c}(\tilde{\boldsymbol{x}}^*)))^T(\boldsymbol{x} - \tilde{\boldsymbol{x}}^*) \geq 0, \forall \boldsymbol{x} \in \Omega_1, \tag{18}$$

which, by Lemma 1, implies that:

$$\tilde{\boldsymbol{x}}^* = P_{\Omega_1}[\tilde{\boldsymbol{x}}^* - \hat{\gamma}\boldsymbol{c}(\tilde{\boldsymbol{x}}^*)]. \tag{19}$$

Hence, according to (11), at the DUE, the predicted flow pattern of class-1 player, $\boldsymbol{\pi}^{1,*} = \tilde{\boldsymbol{x}}^*$.

In fact, for any scaling factor $\eta > 0$ and $\hat{\gamma} > 0$,

$$\begin{aligned} P_{\Omega_\eta}[\eta\tilde{\boldsymbol{x}}^* - \hat{\gamma}\boldsymbol{c}(\tilde{\boldsymbol{x}}^*)] &= \arg\min_{\boldsymbol{y}\in\Omega_\eta} \|\boldsymbol{y} - \eta\tilde{\boldsymbol{x}}^* + \hat{\gamma}\boldsymbol{c}(\tilde{\boldsymbol{x}}^*)\|^2 = \arg\min_{\boldsymbol{y}\in\Omega_\eta} \left\| \frac{\boldsymbol{y}}{\eta} - \tilde{\boldsymbol{x}}^* + \frac{\hat{\gamma}}{\eta}\boldsymbol{c}(\tilde{\boldsymbol{x}}^*) \right\|^2 \\ &= \eta \arg\min_{\boldsymbol{y}\in\Omega_1} \left\| \boldsymbol{y} - \tilde{\boldsymbol{x}}^* + \frac{\hat{\gamma}}{\eta}\boldsymbol{c}(\tilde{\boldsymbol{x}}^*) \right\|^2 = \eta\tilde{\boldsymbol{x}}^*. \end{aligned} \tag{20}$$

Applying (20) to the definition of the 2-step travelers' predicted cost in (12), we obtain that the predicted flow pattern of class-2 player, $\boldsymbol{\pi}^{2,*} = \tilde{\boldsymbol{x}}^*$.

Summarizing the above, the predicted flow patterns of all the three classes at DUE are exactly $\tilde{\boldsymbol{x}}^*$, and thus (14) becomes (16). □

3.2 Local stability

The MPE's non-uniqueness makes global stability analysis difficult, if not impossible, because we cannot construct a global convex Lyapunov function that decreases as time passes. We, therefore, turn to analyze its local stability. The definitions and theorems on local stability used in this paper are relegated to the Appendix A. In this subsection, we first give the Jacobian of the CH-NTP dynamic at the MPE and then analyze the stability near the DUE.

3.2.1 Jacobian matrix

The following lemma describes the property of the Jacobian matrix of a projection operator.

Lemma 2. *For a projection of a vector $\boldsymbol{z}$ onto $\Omega_\eta \equiv \{\boldsymbol{x}|\Gamma\boldsymbol{x} = \eta\boldsymbol{d}, \boldsymbol{x} \geq 0\}$, its Jacobian is a diagonal block matrix:*

$$Q[\boldsymbol{z}] = \begin{bmatrix} Q_{w=1}[\boldsymbol{z}_1] & & \mathbf{0} \\ & \ddots & \\ \mathbf{0} & & Q_{w=|W|}\left[\boldsymbol{z}_{|W|}\right] \end{bmatrix}, \tag{21}$$

with each block element $Q_w[\boldsymbol{z}_w]$ being $Diag(\mathbb{1}_w) - \frac{\mathbb{1}_w\mathbb{1}_w^T}{|E(\boldsymbol{z}_w)|}$, where $\mathbb{1}_w$ is an indicator vector of size $|R_w|$ whose r-th entry is 1 if $r \in E(\boldsymbol{z}_w)$ and 0 otherwise. $E(\boldsymbol{z}_w)$ is the set of routes on w that exhibit positive flow after applying the operator onto $\Omega_\eta^w \equiv \{\boldsymbol{x}|\Gamma_w\boldsymbol{x} = \eta d_w, \boldsymbol{x} \geq 0\}$, where Γ_w is the OD-incidence matrix of OD pair w. Each $Q_w[\boldsymbol{z}_w]$ is positive semidefinite (PSD) whose eigenvalues are either 0 or 1. It is also idempotent; i.e., $(Q_w[\boldsymbol{z}_w])^n = Q_w[\boldsymbol{z}_w], \forall n \in \mathbb{N} = \{1, 2, \ldots\}, \forall w$. $Rank(Q_w[\boldsymbol{z}_w]) = tr(Q_w[\boldsymbol{z}_w]) = |E(\boldsymbol{z}_w)| - 1$. It has a repeated eigenvalue 1 with an algebraic and geometric multiplicity of both $|E(\boldsymbol{z}_w)| - 1$. $Rank(Q_w[\boldsymbol{z}_w] - I) = |R_w| - |E(\boldsymbol{z}_w)| + 1$.

If the projected vector lies in the interior of $\Omega_\eta^w, \forall w$ (i.e., all the route flows after projection are positive), $Q[\boldsymbol{z}]$ degrades to $\bar{Q}$ with each block of OD pair w being $\bar{Q}_w = Diag(\mathbf{1}_w) - \frac{\mathbf{1}_w\mathbf{1}_w^T}{|R_w|}$ where $\mathbf{1}_w$ is an all-one vector of size $|R_w|$.

Proof. See Appendix B. □

Remark 1. *The algebraic and geometric multiplicities of $Q[\boldsymbol{z}]$ in Lemma 2 are used to identify the local stability (instead of local asymptotic stability) when the Jacobian matrix has eigenvalue(s) of 1; see the requirement of the Jordan block of order 1 in condition (ii) of Theorem A.1.*

With Lemma 2, the Jacobian matrix for the CH-NTP dynamic can be derived as follows and used to examine the local stability at any MPE by checking its eigenvalues.

Fact 1. *The Jacobian matrix for the CH-NTP dynamic with $|K| = 3$ is a 3-by-3 block matrix:*

$$JP = \begin{bmatrix} JP_{0,0} & JP_{0,1} & JP_{0,2} \\ JP_{1,0} & JP_{1,1} & JP_{1,2} \\ JP_{2,0} & JP_{2,1} & JP_{2,2} \end{bmatrix}, \tag{22}$$

where each block $JP_{i,j}$ is defined as follows.

$$
\begin{aligned}
JP_{0,0} &= \alpha Q_0 \cdot (I - \gamma D_0) + (1-\alpha)I, \\
JP_{0,j\neq 0} &= \alpha Q_0 \cdot (-\gamma D_0), \\
JP_{1,1} &= \alpha Q_1 \cdot \Big(I - \gamma\Big(D_1 \cdot (\hat{\alpha}\hat{Q}_1^0 \cdot (I - \hat{\gamma} D_0) + (1-\hat{\alpha})I)\Big)\Big) + (1-\alpha)I, \\
JP_{1,j\neq 1} &= \alpha Q_1 \cdot \Big(-\gamma\Big(D_1 \cdot (\hat{\alpha}\hat{Q}_1^0 \cdot (I - \hat{\gamma} D_0) + (1-\hat{\alpha})I)\Big)\Big), \\
JP_{2,2} &= \alpha Q_2\Big(I - \gamma D_2\Big[\hat{\alpha}\hat{Q}_2^0(q_2^0 I - \hat{\gamma} D^0) + (1-\hat{\alpha})I + \hat{\alpha}\hat{Q}_2^1\Big(q_2^1 I - \hat{\alpha}\hat{\gamma} D_1\Big(\hat{\alpha}\hat{Q}_1^0(I - \hat{\gamma} D_0) + (1-\hat{\alpha})I\Big)\Big)\Big]\Big) + (1-\alpha)I, \\
JP_{2,j\neq 2} &= \alpha Q_2\Big(-\gamma D_2\Big[\hat{\alpha}\hat{Q}_2^0(q_2^0 I - \hat{\gamma} D^0) + (1-\hat{\alpha})I + \hat{\alpha}\hat{Q}_2^1\Big(q_2^1 I - \hat{\alpha}\hat{\gamma} D_1\Big(\hat{\alpha}\hat{Q}_1^0(I - \hat{\gamma} D_0) + (1-\hat{\alpha})I\Big)\Big)\Big]\Big),
\end{aligned}
$$

where $D_k \equiv D\left[\boldsymbol{\pi}^{k,(t+1)}\right]$ representing the Jacobian of the route cost functions evaluated at $\boldsymbol{\pi}^{k,(t+1)}$; $Q^k \equiv Q\left[\boldsymbol{x}^{k,(t)} - \gamma \boldsymbol{c}\left(\boldsymbol{\pi}^{k,(t+1)}\right)\right]$; I the identity matrix of size $\sum_w |R_w|$; and $\hat{Q}_1^0 \equiv Q\left[q_1^0 \tilde{\boldsymbol{x}}^{(t)} - \hat{\gamma}\boldsymbol{c}\left(\boldsymbol{\pi}^{0,(t+1)}\right)\right]$, $\hat{Q}_2^0 \equiv Q\left[q_2^0 \tilde{\boldsymbol{x}}^{(t)} - \hat{\gamma}\boldsymbol{c}\left(\boldsymbol{\pi}^{0,(t+1)}\right)\right]$, $\hat{Q}_2^1 \equiv Q\left[q_2^1 \tilde{\boldsymbol{x}}^{(t)} - \hat{\gamma}\boldsymbol{c}\left(\boldsymbol{\pi}^{1,(t+1)}\right)\right]$.

Proof. The derivation is relegated to Appendix C. □

As stated in Section 3.1, the strategic-reasoning behavior causes the original NTP dynamic to have multiple MPE, including those non-DUE ones. Local stability regarding all the MPE can be analyzed by the Jacobian in Fact 1.

3.2.2 Stability around the DUE

We are particularly interested in how the travelers' prediction behaviors would affect the stability near the DUE. Numerically, it is always tractable to calculate JP's eigenvalues at the DUE and check its local stability. However, general analytical insights on the parametric space may rely on certain assumptions. Recognizing this, we assume that as the day-to-day process evolves, the projection always yields a positive flow on each route. Under this assumption, the NTP dynamic reduces to a closed-form expression (Sandholm, 2010; Xiao et al., 2016). The α and γ (and $\hat{\alpha}$ and $\hat{\gamma}$) can be simply combined (specifically, multiplied) to represent the sensitivity to the cost difference between two routes; see Appendix A in Xiao et al. (2016). We can therefore fix $\alpha = \hat{\alpha} = 1$ and vary γ and $\hat{\gamma}$ while the behavioral explanation is not compromised.

We divide the discussion into two parts: (i) when higher-step travelers can exactly predict lower-step travelers' switching tendency, i.e., $\hat{\gamma} = \gamma$; and (ii) when the prediction is inaccurate, i.e., $\hat{\gamma} \neq \gamma$.

The following assumption is made on the route cost function when analyzing the stability around the DUE.

Assumption 1. *The Jacobian of the route cost function $\boldsymbol{c}(\boldsymbol{x})$ w.r.t. route flow pattern $\boldsymbol{x} \in \Omega_1$, denoted by $D[\boldsymbol{x}]$, is symmetric and positive semidefinite.*

A widely-adopted case of Assumption 1 is when link travel time functions are separable, differentiable, increasing, and additive (i.e., the route travel time is equal to the sum of travel time on all links that constitute the route).

3.2.2.1 Perfect prediction $\hat{\gamma} = \gamma$

Proposition 3. *For a dynamical system* (9)-(12) *featuring any $|K| \in \{1, 2, 3\}$, if the projection operator can always generate positive flow on each route (hence $\hat{\alpha}$ and α can be set to 1) and $\hat{\gamma} = \gamma$, its DUE under Assumption 1 is locally stable if all the moduli of the eigenvalues of matrix $\bar{Q}(I - \gamma D_*)$ are less than 1, where D_* is the Jacobian of the route cost function evaluated at the aggregate DUE, $\tilde{\boldsymbol{x}}^*$, and $\bar{Q}$ is defined in Lemma 2.*

Proof. See Appendix D. □

Remark 2. *Proposition 3 shows that conditions for ensuring local stability near the DUE are equivalent for any $|K| \in \{1, 2, 3\}$ when $\hat{\gamma} = \gamma$. In other words, thinking multiple steps ahead does not affect the local stability at the DUE when higher-step travelers can exactly predict lower-step ones' switching behavior. Moreover, the stability is independent of the distribution of heterogeneous travelers.*

The difference between models with different $|K|$ is that (as we shall see in the numerical experiments) the instability condition of $|K| = 1$ leads to a permanent oscillating pattern near the DUE (i.e., crossing the DUE infinitely many times) while for $|K| \geq 2$ it is more likely that the system will evolve to and stick at an MPE that is not DUE.

The following lemma describes the property of the stability criterion used in Proposition 3, $Q[\boldsymbol{z}](I - \gamma D[\boldsymbol{x}])$, by relating it to the PSD matrix $Q[\boldsymbol{z}]D[\boldsymbol{x}]$, where $Q[\boldsymbol{z}]$ and $D[\boldsymbol{x}]$ are not necessarily equal to $\bar{Q}$ and D_*, respectively.

Lemma 3. *Under Assumption 1, for any given $\boldsymbol{z}$ and $\boldsymbol{x}$, denote μ_i as $Q[\boldsymbol{z}]D[\boldsymbol{x}]$'s i-th eigenvalue and $\mu_i \geq 0, \forall i$. The corresponding eigenvalue of $Q[\boldsymbol{z}](I - \gamma D[\boldsymbol{x}])$ is $1 - \gamma\mu_i$ if $\mu_i \neq 0$. Therefore, as γ increases from 0 to ∞, the modulus of the i-th eigenvalue of $Q[\boldsymbol{z}](I - \gamma D[\boldsymbol{x}])$, $|1 - \gamma\mu_i|$, will first decrease*

from 1 *to* 0 *and then increase to* ∞. *As a result, there exists a* $\bar{\gamma} = \frac{2}{\max_i \mu_i}$ *such that when* $\gamma < \bar{\gamma}$, *the maximum modulus* $\max_i |1 - \gamma\mu_i| < 1$ *and that when* $\gamma > \bar{\gamma}$, $\max_i |1 - \gamma\mu_i| > 1$.

Proof. See Appendix E. □

3.2.2.2 Imperfect prediction when $|K| = 2$

The consistency of stability conditions under different $|K|$ breaks down when $\hat{\gamma} \neq \gamma$. We first turn to analyze a simple toy network to get some intuitions. Consider an OD pair served by two routes with $|K| = 2$. According to Proposition 2, at the DUE, $\boldsymbol{\pi}^{0,(t+1)} = \boldsymbol{\pi}^{1,(t+1)}$ and thus the Jacobians of route cost function $D_1 = D_0 = D_*$. Without loss of generality, we assume $D_* = \left[\begin{smallmatrix} a & b \\ b & c \end{smallmatrix}\right]$ with $a, b, c > 0$ and $ac - b^2 \geq 0$ (positive semidefiniteness in Assumption 1). Using the similar derivation in Proposition 3, we can obtain that JP with $|K| = 2$ has four eigenvalues 0, 0, 1 and $\frac{1}{4}\gamma\hat{\gamma}(a - 2b + c)^2 - \gamma(a - 2b + c) + 1$, with the last one being denoted as $f(a - 2b + c; \gamma, \hat{\gamma})$. Note that the stability only depends on $f(a - 2b + c; \gamma, \hat{\gamma})$ and that $a - 2b + c \geq 0$ because $ac - b^2 \geq 0$. We refer to stable/unstable region as region of γ and $\hat{\gamma}$ that makes the DUE stable/unstable (i.e., whether $f(a - 2b + c; \gamma, \hat{\gamma}) \in (-1, 1)$ holds or not).

The following observations can be made:

- When $\hat{\gamma} = \gamma$, $-1 < f(a - 2b + c; \gamma, \hat{\gamma}) < 1$ simplifies to $a - 2b + c < \frac{4}{\gamma}$.
- When $\hat{\gamma} > \gamma$, the stable region is still $a - 2b + c < \frac{4}{\hat{\gamma}}$. Compared to the case of $\hat{\gamma} = \gamma$, the size of the stable region is shrunk.
- When $\frac{\gamma}{2} < \hat{\gamma} < \gamma$, the minimum point of $f(a - 2b + c; \gamma, \hat{\gamma})$, $1 - \frac{\gamma}{\hat{\gamma}}$, is always > -1. Since the zero points of $f(a - 2b + c; \gamma, \hat{\gamma}) = 1$ are 0 and $\frac{4}{\hat{\gamma}}$, respectively, the stable region becomes $a - 2b + c < \frac{4}{\hat{\gamma}}$. Compared to the case of $\hat{\gamma} = \gamma$, the size of the stable region expands because $\hat{\gamma} < \gamma$.
- When $\hat{\gamma} < \frac{\gamma}{2}$, $f(a - 2b + c; \gamma, \hat{\gamma}) = -1$ will have two zero points. The stable region is separated. One region ranges from 0 to the first zero point, $2\hat{\gamma} - \frac{2\sqrt{\gamma(\gamma - 2\hat{\gamma})}}{\gamma\hat{\gamma}}$, and the other ranges from the second zero point, $2\hat{\gamma} + \frac{2\sqrt{\gamma(\gamma - 2\hat{\gamma})}}{\gamma\hat{\gamma}}$, to $\frac{4}{\hat{\gamma}}$. The combined size of these two regions is $\frac{4}{\hat{\gamma}} - \frac{4\sqrt{\gamma(\gamma - 2\hat{\gamma})}}{\gamma\hat{\gamma}}$. By the inequality of arithmetic and geometric means and after algebraic simplification, we can see that $\frac{4}{\hat{\gamma}} - \frac{4\sqrt{\gamma(\gamma - 2\hat{\gamma})}}{\gamma\hat{\gamma}} \geq \frac{4}{\gamma}$. Hence, the total size of the two separated regions is increased.

The above discussion shows that when higher-step travelers over-predict lower-step ones' switching tendency, the stability condition is more restricted. In contrast, a "mild" under-prediction helps relax the stability condition.

Although revealed by a simple two-route network, the above finding still holds in general networks, as shown in the following proposition.

Proposition 4. *Consider a dynamical system* (9)-(11) *with* $|K| = 2$ *where the projection can always generate positive flow on each route (hence* $\hat{\alpha}$ *and* α *can be set to 1). Denote* β_i *as* $\bar{Q}D_*$*'s i-th eigenvalue and* $\beta_i \geq 0, \forall i$*. The DUE is locally stable if and only if* $\left|\gamma\hat{\gamma}\beta_i^2 - 2\gamma\beta_i + 1\right| < 1, \forall i$*.*

Proof. See Appendix F. □

Remark 3. *Solving* $\left|\gamma\hat{\gamma}\beta_i^2 - 2\gamma\beta_i + 1\right| < 1$ *for the quadratic function of* β_i *with parameters* γ *and* $\hat{\gamma}$ *generates the same conclusion on how over- and under-predictions affect stability as the simple two-route-network example.*

Moreover, when $\hat{\gamma}$ *is greater than* $\bar{\gamma} = \frac{2}{\max_i \beta_i}$ *defined in Lemma 3,* $\max_i \beta_i > \frac{2}{\hat{\gamma}}$*. Since the right root of* $\gamma\hat{\gamma}\beta_i^2 - 2\gamma\beta_i + 1 = 1$ *is* $\frac{2}{\hat{\gamma}}$*, the quadratic equation is always greater than 1 when* $\hat{\gamma} > \bar{\gamma}$ *and thus the system with* $|K| = 2$ *is always unstable, regardless of* γ*.*

4 Validation Using a Virtual Experiment

Ye et al. (2018) conducted an online route choice experiment to mimic travelers' decision-making processes from day to day. The experiment collected 268 participants' route choices on 26 rounds, where each round corresponded to a true calendar day. It was conducted on the well-known Braess paradox network (Figure 1) with one OD pair served by three routes: Route 1 as $1 \to 3 \to 5$; Route 2 as $2 \to 5 \to 3$; and Route 3 as $2 \to 4$. The travel time on each link $a \in L$ was given by the well-known BPR function: $t_a(v_a) = t_a^0\left(1 + 0.15\left(\frac{v_a}{V_a}\right)^4\right)$, with parameters marked in the figure in order as $(a,\ t_a^0,\ V_a)$, where t_a^0 is the free-flow travel time and V_a the capacity. The observed route flow (i.e., how many participants selected that route) on each day is visualized in Figure 2 with the days indexed from 0 to 25. Note the large oscillations in the trajectories in Figure 2. Readers can refer to Ye et al. (2018) for more details of the experiment.

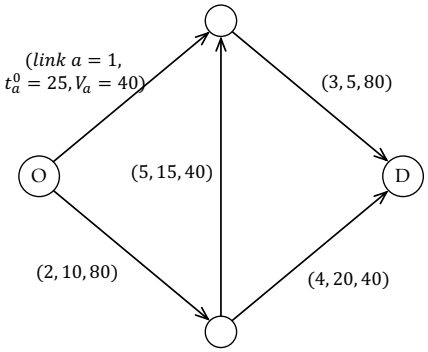

Figure 1: Braess network used in the virtual experiment (Ye et al., 2018).

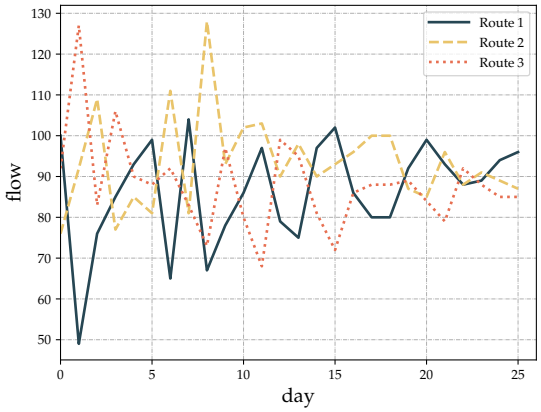

Figure 2: Collected route flow evolutions in the virtual experiment (Ye et al., 2018).

4.1 Difficulty of prevailing models without prediction in reproducing the observed pattern

A natural way of calibrating a day-to-day dynamical model is to find the optimal parameters that minimize the sum of squared error between simulated and observed flow evolution trajectories. In doing so, Ye et al. (2018) found that the prevailing day-to-day models could not produce fluctuated trajectories fitting the experimental data; see Figure 3 of that paper. (Due to the intractability of the above "simulation-based" method, they had to turn to a relaxed problem using regression analysis.) Below we give an explanation of the prevailing models' difficulties.

To explain, we plot the net flow of three routes on each day t in Figure 3. We use different colors and shapes to mark different routes ranked by the travel cost on the day $t-1$: green square points for the shortest route, yellow triangular points for the second-shortest route, and red circular points for the longest route.

First note that for day $t \in [1, 16]$, the longest route on the day $t-1$ would by-and-large out-flow to the other two routes on the day t. This observation is in line with most day-to-day models' assumption that travelers would select the routes with lower costs. However, there was no distinction between the shortest and the second-shortest routes. On quite a few days (i.e., 1, 3, 8, 9, 10, and 13), the previous day's second-shortest route received more inflow than the shortest route. This indiscrimination between the shortest and the second-shortest routes contradicted the best-response-based day-to-day models' underlying hypothesis that the shortest route would be the most popular (e.g., Friesz et al., 1994; He et al., 2010; Xiao et al., 2016). We argue that this indiscrimination was a consequence of strategic thinking. Specifically,

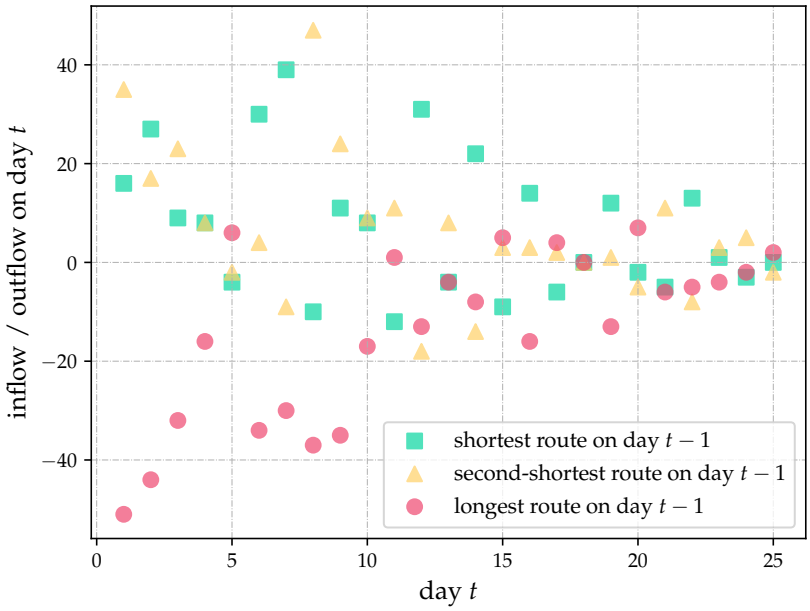

Figure 3: Net flow on day t for the three routes sorted by travel cost on day $t-1$ in the virtual experiment.

a 1-step traveler might think that other travelers would go for the shortest route of the day $t-1$ and thus avoided switching to that route on the day t. As a result, the second-best route becomes her preference.

For day $t \in [17, 25]$, a keen-eyed reader may find that travelers' preferences seem to become independent of yesterday's route flow pattern. For example, the net in- and out-flows of the three routes on day 18 are 0, regardless that the DUE had not been achieved. We conjecture that the participants learned after 18 days' experience that the occurrence of the shortest route was highly non-predictable and hence used a uniformly-random mixed strategy to respond. (We learned this phenomenon from conversations with some participants in the final days.)

Calibration results of our proposed hierarchical model confirm the above discussions, which are presented in the sub-sections to follow.

4.2 Calibrations of the CH-NTP dynamic

To minimize the number of parameters, we consider special cases with perfect prediction (i.e., $\hat{\gamma} = \gamma$) and $\hat{\alpha} = \alpha = 1$. By doing so, we intend to demonstrate our model's general explanation capability rather than "overfit" data using more parameters. (Relaxing these constraints will further reduce the fitting errors.) The 0-step model is exactly the so-called XYY dynamics used

in Xiao et al. (2016) and Ye et al. (2018), which has only one parameter, γ, to be estimated. (The other day-to-day models (without prediction) calibrated in Ye et al. (2018) exhibited very similar (bad) performance as the 0-step model and hence are omitted here for simplicity. We aim to show how introducing cognitive hierarchy can significantly improve model interpretation.) The 1-step model has one more parameter p^0 because p^1 equals $1 - p^0$. And the 2-step model has three parameters, namely, γ, p^0, and p^1.

4.2.1 Preparations

We conducted calibration by minimizing the root mean square error (RMSE) between the predicted flows and the ground truth:

$$RMSE = \sqrt{\frac{\sum_{t=1}^{M}\sum_{r=1}^{3}\left(\hat{x}_r^{(t)} - \bar{x}_r^{(t)}\right)^2}{3M}}, \tag{23}$$

where M is the number of days (i.e., days 1 to M) used for calibration, $\hat{x}_r^{(t)}$ is the model-predicted aggregate flow on route r of day t, and $\bar{x}_r^{(t)}$ is the observed flow. The RMSE function may be highly non-linear. To avoid being trapped in local optima, we performed a grid search over the parametric space with γ varying from 0.01 to 1.0 with step 0.002, p^0 and p^1 ranging from 0.01 to 1.0 with step 0.01. For models with $|K| \geq 2$, given all the parameters, the initial route flow pattern (on day 0) was chosen such that the predicted aggregate route flow pattern on day 1 was closest to the observed one in terms of RMSE.

For each CH-NTP dynamic with different $|K|$, the optimal parameters that minimize the RMSE function (23) are used to calculate log-likelihoods and perform likelihood ratio tests. The log-likelihood function is derived as follows. We can first obtain a k-step traveler's probability of choosing a particular route by dividing the route flow of k-step travelers by their OD demands. Denote $g^k\left(r_l^{j,(t)} \mid \gamma, p^0, \ldots, p^{|K|-1}\right)$ as the model's predicted probability of a traveler l from class k choosing route j on day t. Then the final total predicted probability, $G^{(t)}(r_l^j)$, is an aggregation of all thinking steps weighted by the proportions; i.e., $G^{(t)}(r_l^j) = \sum_k p^k g^k\left(r_l^{j,(t)} \mid \gamma, p^0, \ldots, p^{|K|-1}\right)$. Finally, we can form a log-likelihood function by combining all the travelers on all the routes and days:

$$LL\left(\gamma, p^0, \ldots, p^{|K|-1}\right) = \sum_{t=1}^{M}\sum_{l=1}^{268}\sum_{j=1}^{3} I\left(r_i^{j,(t)}\right) \cdot \ln G^{(t)}\left(r_i^j\right), \tag{24}$$

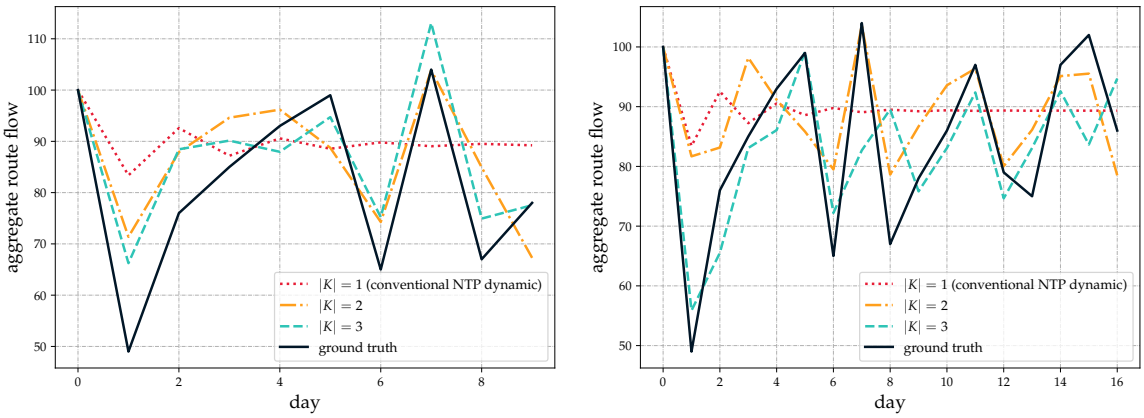

(a) the first 9 days

(b) the first 16 days

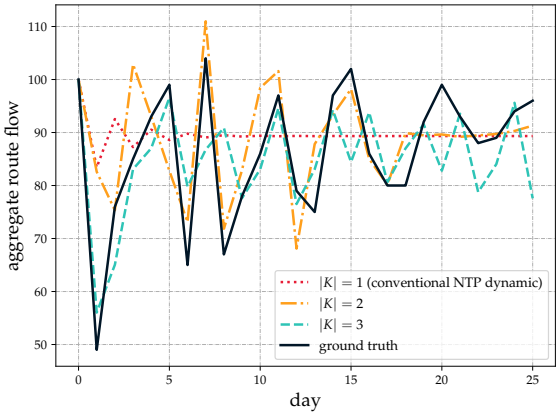

(c) all the 25 days

Figure 4: Comparisons between the calibrated and ground-truth flow evolutions of Route 1.

where $I\left(r_l^{j,(t)}\right)$ is the indicator function being 1 if traveler l chooses route j on day t and 0 otherwise.

4.2.2 Results

The simulated flow evolutions of Route 1 with the parameters that minimized the RMSE are presented in Figures 4a-c for $M = 9$, 16, and 25, respectively. (The other two routes exhibit similar results and hence are omitted to conserve space.) The likelihood ratio test is reported in Table 1 with the optimal parameters.

First note that in all the figures, the nonhierarchical model with $|K| = 1$, i.e., the conventional NTP dynamic, fails to produce a significant fluctuation pattern fitting the ground-truth trajectory; see the dotted curves. This result is in agreement with Ye et al. (2018). The corresponding flow trajectories for $M = 9$, 16, and 25 are identical and the optimal $\gamma = 0.358$.

Further note that we have previously implemented a multi-class day-to-day model where

Table 1: Calibration results of the CH-NTP dynamic

Number of days		9			16			25	
CH-NTP dynamic with $\|K\|$ =	1	2	3	1	2	3	1	2	3
Estimated log-likelihood$^{\diamond}$	-2646.2	-2631.3	-2618.8	-4706.1	-4693.8	-4680.2	-7356.0	-7344.3	-7334.4
Maximum log-likelihood*		-2604.0			-4652.6			-7297.7	
Likelihood Ratio Test	-	29.8	52.8	-	24.5	51.7	-	23.3	43.0
p-value	-	4.77-e8	1e-12	-	7.58-e7	6e-12	-	1.35e-6	4.62e-10
γ	0.358	0.708	0.522	0.358	0.570	0.508	0.358	0.566	0.492
Parameters p^0	-	0.88	0.37	-	0.94	0.31	-	0.90	0.31
p^1	-	-	0.23	-	-	0.05	-	-	0.05

$^{\diamond}$ Estimated log-likelihood using the optimal parameters that minimized RMSE function (23).
* The maximum that the Log-likelihood function can achieve, i.e., the entropy of the ground-truth route choice distribution.

each class is associated with a distinct sensitivity parameter (Zhou et al., 2020). Despite increasing the number of classes to three, this multi-class model still fails to reproduce the observed fluctuation pattern. In fact, the calibrated flow evolution from this model closely resembles the pattern seen in the $|K| = 1$ case (illustrated by the red dotted curve in Figures 4a-c). This outcome strongly suggests that our improved fitting performance is not merely a result of additional parameters, but rather stems from the enhanced explanatory capability of our proposed model.

Happily, significant fluctuation patterns emerge when some travelers think one step further, as revealed by the yellow dash-dotted curves. The fitting error decreases as a consequence. Note in Figures 4b and c how the predicted curves faithfully capture the ground-truth trend from day 5 to 16. This is also confirmed by observing that the hierarchical model of $|K| = 2$ improves the log-likelihood by 24.5 and 23.3 for $M = 16$ and 25, respectively. Moreover, the hierarchical model with $|K| = 3$ almost doubles the log-likelihood improvement and exhibits better fitting performance from the very first day until day 16. All the improvements are statistically significant under the likelihood ratio test with the p-value less than 0.0002%.

Fitting performance is less satisfying for days 17-25, as shown by the trailing edges of the curves in Figure 4c. A possible reason is that as the experiment proceeded, the participants found themselves gaining little by predicting the population's behaviors and thus exhibited somehow uniformly-random behaviors in the last eight days (see the explanations on this matter in Section 4.1). Our time-invariant parameters cannot capture such a pattern.

5 Numerical Experiments

In this section, we conduct numerical experiments to verify the previous sections' theoretical results and highlight some features not captured by the theoretical analysis.

5.1 Evolutions towards multiple equilibria

We examine how the strategic-reasoning behavior leads the system to multiple equilibria. We use the Braess network in the virtual experiment as our first example. At the DUE, the aggregate route flow pattern is $(89.33, 89.33, 89.33)^T$. We set $p^0 = p^1 = 0.5$ ($|K| = 2$), $\hat{\alpha} = \alpha = 0.3$, $\hat{\gamma} = \gamma$. Figures 5a and b depict the evolution trajectories in terms of aggregate route flow on each route, starting from different initial points (distinguished by different colors) for $\gamma = 1.4$ and 0.2, respectively. (Plotting two routes is sufficient as the degree of freedom is only two due to the flow conservation constraint.) At the initial point, all the routes share the same p^0 and p^1.

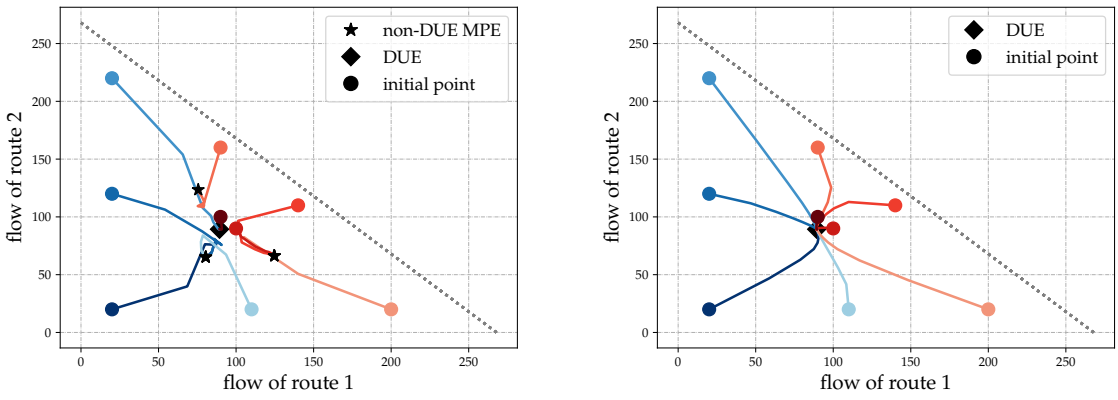

(a) $\gamma = 1.4$ (b) $\gamma = 0.2$

Figure 5: Evolutions of route flows starting from different initial route flow patterns under different $\gamma = \hat{\gamma}$ for $|K| = 2$. $p^0 = p^1 = 0.5$, $\hat{\alpha} = \alpha = 0.3$.

First note in Figure 5a how different initial points result in different evolution trajectories and steady states under a large γ. It is interesting to see that two initial points close to each other can evolve to totally different equilibrium points, as shown by the two trajectories starting in the middle. This kind of multiple-equilibria phenomenon is rooted in travelers' strategic-thinking behaviors rather than the asymmetry of the travel cost functions previously studied in the literature (see, e.g., Watling, 1996; Bie and Lo, 2010; Han et al., 2017). We believe this system feature would enrich behavioral explanation capability.

Things change a lot when γ is small. With a small γ, travelers are reluctant to switch to

shorter routes and tend to believe other travelers are also conservative (as $\hat{\gamma}$ is set to equal γ). As a consequence, all the initial points will gradually evolve to the DUE, as shown in Figure 5b.

5.2 Local stability near the DUE

We next test stability conditions on a larger network used in Zhang et al. (2015); see Figure 6. It contains 8 routes that connect two OD-pairs with demand $(90, 90)^T$: Route 1 as $1 \rightarrow 9 \rightarrow 14$; Route 2 as $1 \rightarrow 5 \rightarrow 10$; Route 3 as $2 \rightarrow 6 \rightarrow 10$; Route 4 as $2 \rightarrow 11 \rightarrow 15$; Route 5 as $3 \rightarrow 11 \rightarrow 16$; Route 6 as $3 \rightarrow 7 \rightarrow 12$; Route 7 as $4 \rightarrow 8 \rightarrow 12$; and Route 8 as $4 \rightarrow 13 \rightarrow 17$. Link travel times are again given by the well-known BPR function with link numbers, free-flow travel times, and capacities marked in the figure in order as $(a,\ t_a^0,\ V_a)$. The aggregate DUE is $(20, 20, 25, 25, 25, 25, 20, 20)^T$.

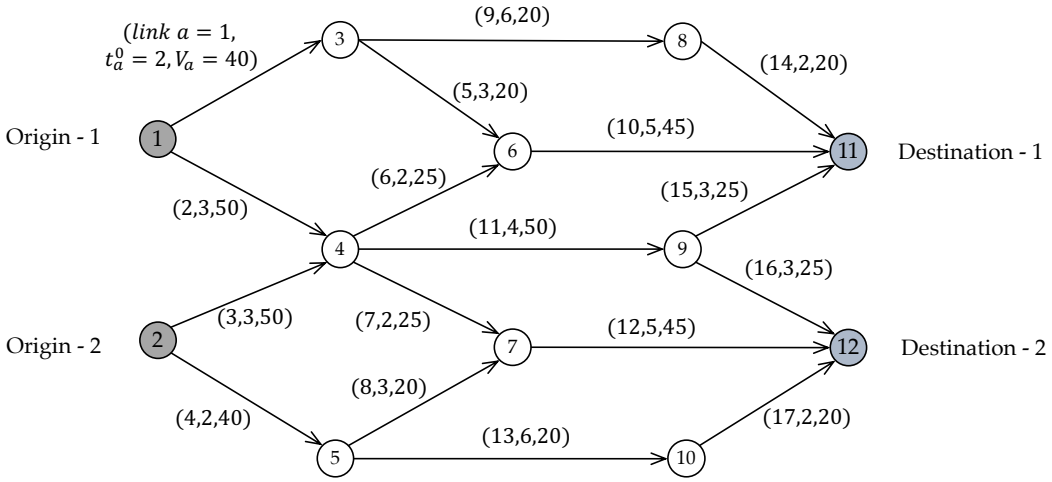

Figure 6: A larger testing network (from Zhang et al., 2015).

5.2.1 In the interior of the feasible route flow set

We first assess Proposition 3 where predictions can be perfectly made, and the projection operators yield positive flows on all the routes. Since we focus on the local stability, the initial aggregate route flow pattern in the following experiments is slightly perturbed from the DUE. We set $p^0 = 0.4, p^1 = 0.6$ for all the routes at the initial point, $\hat{\alpha} = \alpha = 1.0$ and $\hat{\gamma} = \gamma$. We calculate that $\bar{\gamma} \approx 0.79$ in Lemma 3. According to Proposition 3 and Lemma 3, the equilibrium is stable when $\gamma < \bar{\gamma}$ and unstable when $\gamma > \bar{\gamma}$. Figures 7a and b plot two selected routes' flow trajectories for $\gamma = 0.78$ and 0.8, respectively. It is expected that for both $|K| = 1$ and 2, a smaller $\gamma(= 0.78)$ eliminates the small initial perturbations while a larger $\gamma(= 0.8)$ renders the

system deviating from the DUE. Note that for $|K| = 1$, such a deviation results in a permanent oscillation near the DUE, while for $|K| = 2$, the system evolves to a new MPE that is not DUE.

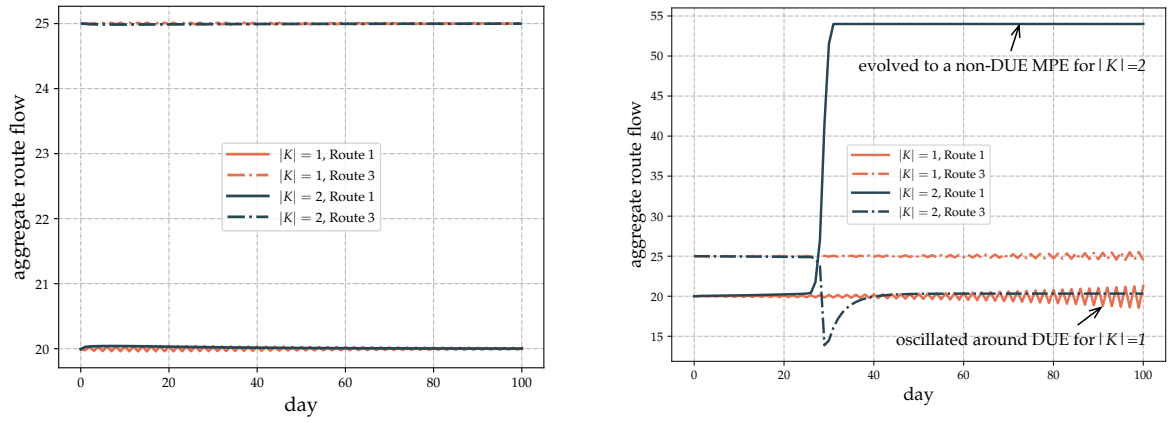

(a) $\gamma = 0.78$ (b) $\gamma = 0.8$

Figure 7: Flow evolutions of the CH-NTP dynamic with $|K| \in \{1, 2\}$ under different γ.

We now verify Proposition 4 where predictions are inaccurate. All the parameters and initial flow patterns are the same as the above case except for the values of γ and $\hat{\gamma}$. Figure 8 depicts whether or not the system deviates from the DUE after a small perturbation for various combinations of γ and $\hat{\gamma}$ in a resolution of 0.05, where solid circles and crosses denote stable and unstable systems, respectively. The points on the 45° solid curve represent the case of $\hat{\gamma} = \gamma$ (perfect prediction), and the solid curve lying beneath represents the case of $\hat{\gamma} = \frac{\gamma}{2}$. The approximate $\bar{\gamma} = 0.79$ by Lemma 3 is also marked.

First note the green shaded area where a moderately small $\hat{\gamma}$, $\frac{\gamma}{2} < \hat{\gamma} < \bar{\gamma} < \gamma$, helps stabilize the dynamic even when γ exceeds $\bar{\gamma}$. This justifies the finding in Proposition 4 that, a mild under-prediction enlarges the stable region. In contrast, when $\hat{\gamma}$ is very small (i.e., $< \frac{\gamma}{2}$), the stable region is separated into two pieces. The eigenvalues of $\bar{Q}D_*$ that previously satisfy the stability condition when $\hat{\gamma} = \gamma < \bar{\gamma}$ fall into the unstable region due to the separation when $\hat{\gamma} < \frac{\gamma}{2}$; see the red shaded area. In addition, as expected in Remark 3, a $\hat{\gamma} > \bar{\gamma}$ will make the system permanently unstable, regardless of γ; see all the crosses above the horizontal line of $\bar{\gamma} = 0.79$. Finally, for this particular numerical case, although the stable region size is reduced when over-predictions occur ($\gamma < \hat{\gamma} < \bar{\gamma}$), The eigenvalues of $\bar{Q}D_*$ still satisfy the stability condition in Proposition 4 and thus the points above the curve $\hat{\gamma} = \gamma$ are stable.

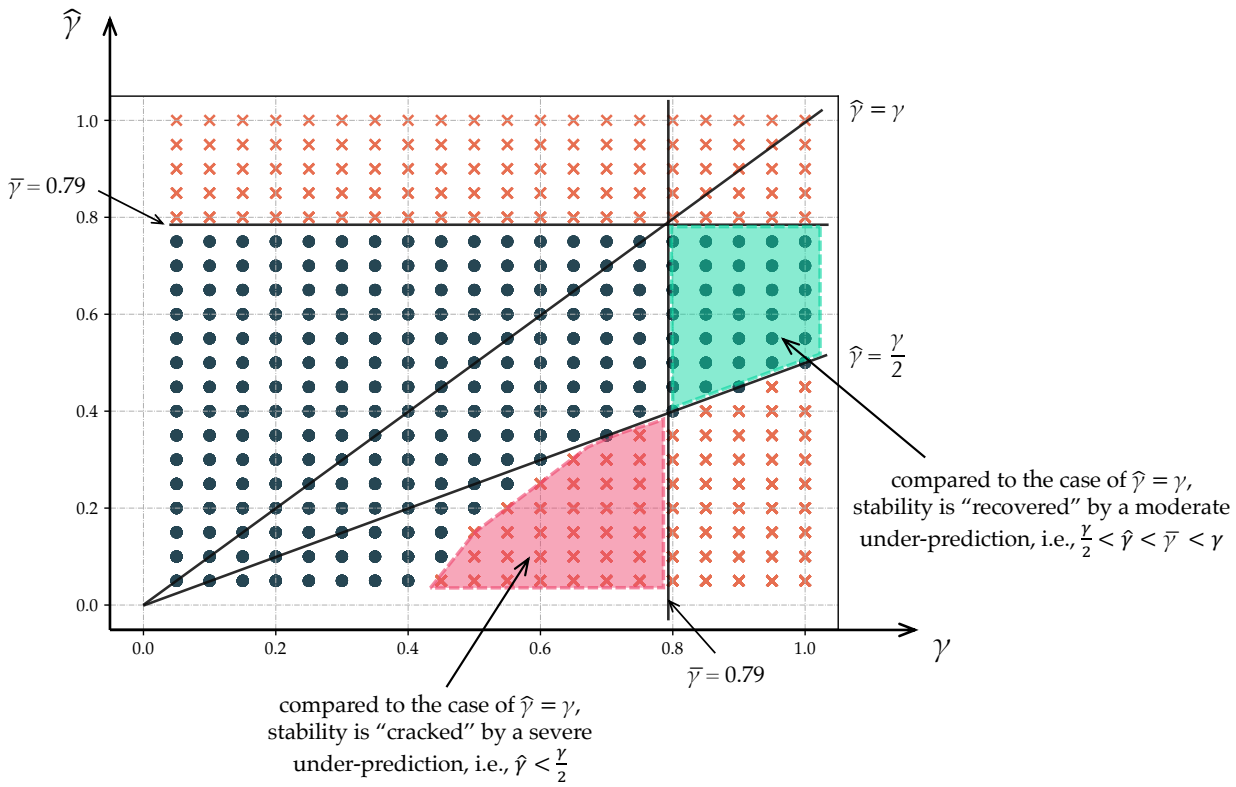

Figure 8: Stable and unstable regions w.r.t. combinations of γ and $\hat{\gamma}$ for the CH-NTP dynamic with $|K| = 2$, $p^0 = 0.4$, $p^1 = 0.6$.

5.2.2 On the boundary of the feasible route flow set

Proposition 3 becomes invalid when the projected flow pattern is on the boundary of the feasible set. Under this circumstance, the general analytical results are invalid, and we have to resort to Fact 1 for numerically checking the stability. To test this fact, we set $|K| = 2$, $\hat{\alpha} = \alpha = 0.5$, $\hat{\gamma} = \gamma \in \{0.81, 0.82\}$, $p^0 = 0.4, p^1 = 0.6$ and the initial route flow pattern as $\boldsymbol{x}^{k=0,(t)=0} = (0, 7.999, 10, 18, 9.98, 10.01, 8.01, 8.01)^T$ and $\boldsymbol{x}^{k=1,(t)=0} = (20, 11.99, 15, 7, 14.98, 15.01, 12.01, 12.01)^T$, such that $JP_{0,0}$ in Fact 1 is evaluated on the boundary. From Fact 1, we have that the maximum moduli of JP of $|K| = 2$ for $\gamma = 0.81$ and 0.82 are 1 and 1.013, respectively. It is expected that the former is stable while the latter is unstable, as shown in Figure 9. The case of $|K| = 3$ is also consistent with the numerical result of Fact 1, which is omitted here for simplicity.

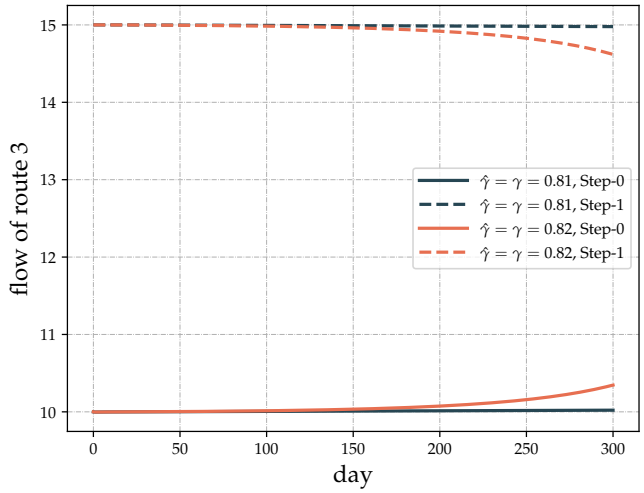

Figure 9: Validation of Fact 1 for $|K| = 2$ when any projected flow is on the boundary of the feasible set.

6 CH-Logit Dynamic

If the day-to-day operator $H[\cdot]$ is replaced by a "stochastic" Logit dynamic (Fudenberg and Levine, 1998; Sandholm, 2010; Xiao et al., 2019), we have the following CH-Logit dynamic:

$$\boldsymbol{x}^{k,(t+1)} - \boldsymbol{x}^{k,(t)} = \alpha\left(p^k \Phi^\theta\left[\boldsymbol{c}\left(\boldsymbol{\pi}^{k,(t+1)}\right)\right] - \boldsymbol{x}^{k,(t)}\right), \tag{25}$$

where $\Phi^\theta[\boldsymbol{z}] \equiv \left(d_w \Phi_w^\theta[\boldsymbol{z}_w], w \in W\right)^T$, $\Phi_w^\theta[\boldsymbol{z}_w] \equiv \left(d_w \varphi_{rw}(\boldsymbol{z}_w), r \in R_w\right)^T$, $\varphi_{rw}(\boldsymbol{z}_w) = \frac{\exp(-\theta z_{rw})}{\sum_{s \in R_w} \exp(-\theta z_{sw})}$, and θ is a dispersal parameter capturing travelers' perception errors. For each $w \in W$, as $\theta \to 0$, choices become equiprobable among all the routes in R_w and as $\theta \to \infty$, choices become extremely concentrated on the least cost route of R_w. Note that for the Logit dynamic, the flow variable (i.e., the first variable) in $\boldsymbol{y}[\cdot]$ of (1) is not explicitly required.

Based on the CH modeling idea in Section 2.3, the predicted flow pattern of each class $k \in \{0, 1, 2\}$ is given by:

$$\boldsymbol{\pi}^{0,(t+1)} = \tilde{\boldsymbol{x}}^{(t)}, \tag{26}$$

$$\boldsymbol{\pi}^{1,(t+1)} = \hat{\alpha} \Phi^{\hat{\theta}}\left[\boldsymbol{c}\left(\boldsymbol{\pi}^{0,(t+1)}\right)\right] + (1 - \hat{\alpha})\tilde{\boldsymbol{x}}^{(t)}, \tag{27}$$

$$\boldsymbol{\pi}^{2,(t+1)} = \hat{\alpha} q_2^0 \Phi^{\hat{\theta}}\left[\boldsymbol{c}\left(\boldsymbol{\pi}^{0,(t+1)}\right)\right] + \hat{\alpha} q_2^1 \Phi^{\hat{\theta}}\left[\boldsymbol{c}\left(\boldsymbol{\pi}^{1,(t+1)}\right)\right] + (1 - \hat{\alpha})\tilde{\boldsymbol{x}}^{(t)}. \tag{28}$$

A significantly large $\hat{\theta}$ can be interpreted as a scenario where higher-step travelers anticipate that lower-step travelers will strongly favor yesterday's shortest path. This situation closely

resembles the case of a large $\hat{\gamma}$ in the CH-NTP model. In both cases, higher-step travelers are making an extreme prediction about the responsiveness of lower-step travelers to cost differences.

6.1 Mixed prediction-based stochastic equilibria

Similar to the case of the CH-NTP dynamic, we term fixed points of the CH-Logit dynamic (25)-(28) as mixed prediction-based stochastic equilibria (MPSE) and describe them in the following proposition.

Proposition 5. *When the route cost function $\boldsymbol{c}(\boldsymbol{x})$ is continuous, the dynamical system* (25)-(28) *admits at least one MPSE (i.e., one fixed point). Moreover, a vector $\boldsymbol{x}^{\circ} \equiv (\boldsymbol{x}^{k,\circ}, k = 0, 1, 2)^T$ is an MPSE if $\forall r \in R_w, w \in W, k \in K$,*

$$x_{rw}^{k,\circ} = p^k d_w \frac{\exp\left(-\theta \pi_{rw}^k(\tilde{\boldsymbol{x}}^{\circ})\right)}{\sum_{s \in R_w} \exp\left(-\theta \pi_{sw}^k(\tilde{\boldsymbol{x}}^{\circ})\right)}, \tag{29}$$

where $\boldsymbol{\pi}^{k,\circ} \equiv (\pi_{sw}^k, s \in R_w, w \in W)^T$ is a function of the aggregate flow pattern $\tilde{\boldsymbol{x}}^{\circ} = \sum_k \boldsymbol{x}^{k,\circ}$, dictated by (26)-(28)*.*

Proof. The existence of a fixed point is guaranteed by the continuities of the closed-form Logit operator and the route cost function. Setting the RHS of (25) to be 0 and rearrange the results yields (29). □

We now give the definition of a $|K|$-class SUE in Definition 2 and show that it is one of the MPSE in Proposition 6 when $\hat{\theta} = \theta$.

Definition 2. *A route flow pattern $\boldsymbol{x}^{\star} \equiv (\boldsymbol{x}^{k,\star}, \boldsymbol{x}^{k,\star} \in \Omega_{p^k}, k \in K)^T$ is said to be a $|K|$-class SUE parameterized by θ if $\forall r \in R_w, w \in W, k \in K$,*

$$x_{rw}^{k,\star} = p^k d_w \frac{\exp\left(-\theta c_{rw}^k(\tilde{\boldsymbol{x}}^{\star})\right)}{\sum_{s \in R_w} \exp\left(-\theta c_{sw}^k(\tilde{\boldsymbol{x}}^{\star})\right)}, \tag{30}$$

where $\tilde{\boldsymbol{x}}^{\star} = \sum_k \boldsymbol{x}^{k,\star}$.

Proposition 6. *When $\hat{\theta} = \theta$, a $|K|(= 3)$-class SUE in Definition 2 parameterized by θ is an MPSE (i.e., a fixed point) of the dynamical system* (25)-(28) *, but not vice versa.*

Proof. At the SUE, first note from (26) that $\boldsymbol{\pi}^{0,\star} = \tilde{\boldsymbol{x}}^{\star}$. Thus, for each $r \in R_w, w \in W$, a 1-step

traveler's predicted flow (27) is:

$$\pi_{rw}^{1,\star} = \hat{\alpha} q_1^0 d_w \frac{\exp\left(-\theta c_{rw}^k(\tilde{\boldsymbol{x}}^\star)\right)}{\sum_{s\in R_w} \exp\left(-\theta c_{sw}^k(\tilde{\boldsymbol{x}}^\star)\right)} + (1-\hat{\alpha}) q_1^0 \tilde{x}_{rw}^\star = \hat{\alpha}\tilde{x}_{rw}^\star + (1-\hat{\alpha})\tilde{x}_{rw}^\star = \tilde{x}_{rw}^\star. \tag{31}$$

where the second equality is due to Definition 2. Accordingly, for each $r \in R_w, w \in W$, a 2-step traveler's predicted flow (28) at the SUE is:

$$\pi_{rw}^{2,\star} = \hat{\alpha}(q_2^0 + q_2^1) d_w \frac{\exp(-\theta c_{rw}^k(\tilde{\boldsymbol{x}}^\star))}{\sum_{s\in R_w} \exp(-\theta c_{sw}^k(\tilde{\boldsymbol{x}}^\star))} + (1-\hat{\alpha})\tilde{x}_{rw}^\star = \tilde{x}_{rw}^\star. \tag{32}$$

Substituting the above predicted costs, $\tilde{\boldsymbol{x}}^\star$, into (25) and by Definition 2, (25) becomes 0. Hence, the SUE is an MPSE.

Similar to the CH-NTP dynamic, there exist some MPSE that are not SUE when $|K| \geq 2$. We can easily construct a counter-example demonstrating their existence (similar to Figure 5a) to negate the necessity. This example is omitted to conserve space. □

6.2 Local stability

Due to the existence of multiple equilibria, this section investigates the CH-Logit dynamic's local stability. We first give the Jacobian of the CH-Logit dynamic at the MPSE and then analyze the stability near the SUE.

6.2.1 Jacobian matrix

Lemma 4. *The Jacobian matrix of the Logit operator parameterized by θ evaluated at a cost vector $\boldsymbol{c}$, $\Upsilon^\theta[\boldsymbol{c}]$, is a block diagonal matrix:*

$$\Upsilon^\theta[\boldsymbol{c}] = \begin{bmatrix} \Upsilon_{w=1}^\theta[\boldsymbol{c}_{w=1}] & & \mathbf{0} \\ & \ddots & \\ \mathbf{0} & & \Upsilon_{w=|W|}^\theta[\boldsymbol{c}_{w=|W|}] \end{bmatrix}, \tag{33}$$

where $\Upsilon_w^\theta[\boldsymbol{c}_w] = -\theta d_w \left(Diag\left(\Phi_w^\theta[\boldsymbol{c}_w]\right) - \Phi_w^\theta[\boldsymbol{c}_w]\left(\Phi_w^\theta[\boldsymbol{c}_w]\right)^T \right)$. Moreover, given any $\boldsymbol{c} \equiv (\boldsymbol{c}_w, w \in W)^T$, each $\Upsilon_w^\theta[\boldsymbol{c}_w]$ is negative semidefinite (NSD), and so is $\Upsilon^\theta[\boldsymbol{c}]$.

Proof. The result for a single w can be obtained from Gao and Pavel (2017) after flipping the positive sign due to the negative utility of travel cost. The independence of routes from different

OD pairs makes the non-diagonal blocks zero. $\Upsilon^{\theta}[\boldsymbol{c}]$ is NSD because a block diagonal matrix is NSD if and only if each diagonal block is NSD. □

With Lemma 4, the Jacobian matrix of Logit dynamic is derived in the following fact.

Fact 2. *The Jacobian matrix for the CH-Logit dynamic with $|K| = 3$ is a 3-by-3 block matrix:*

$$J\Phi = \begin{bmatrix} J\Phi_{0,0} & J\Phi_{0,1} & J\Phi_{0,2} \\ J\Phi_{1,0} & J\Phi_{1,1} & J\Phi_{1,2} \\ J\Phi_{2,0} & J\Phi_{2,1} & J\Phi_{2,2} \end{bmatrix}, \tag{34}$$

where each block $J\Phi_{i,j}$ is defined as follows.

$$\begin{aligned}
J\Phi_{0,0} &= \alpha p^0 \Upsilon^{\theta}_{k=0} D_0 + (1-\alpha) I, \\
J\Phi_{0,j\neq 0} &= \alpha p^0 \Upsilon^{\theta}_{k=0} D_0, \\
J\Phi_{1,1} &= \alpha p^1 \Upsilon^{\theta}_{k=1} D_1 \Big(\hat{\alpha} \Upsilon^{\hat{\theta}}_{k=0} D_0 + (1-\hat{\alpha}) I \Big) + (1-\alpha) I, \\
J\Phi_{1,j\neq 1} &= \alpha p^1 \Upsilon^{\theta}_{k=1} D_1 \Big(\hat{\alpha} \Upsilon^{\hat{\theta}}_{k=0} D_0 + (1-\hat{\alpha}) I \Big), \\
J\Phi_{2,2} &= \alpha p^2 \Upsilon^{\theta}_{k=2} D_2 \Big[\hat{\alpha} q_2^0 \Upsilon^{\hat{\theta}}_{k=0} D_0 + \hat{\alpha} q_2^1 \Phi^{\hat{\theta}}_{k=1} D_1 \Big(\hat{\alpha} \Upsilon^{\hat{\theta}}_{k=0} D_0 + (1-\hat{\alpha}) I \Big) + (1-\hat{\alpha}) I \Big] + (1-\alpha) I, \\
J\Phi_{2,j\neq 2} &= \alpha p^2 \Upsilon^{\theta}_{k=2} D_2 \Big[\hat{\alpha} q_2^0 \Upsilon^{\hat{\theta}}_{k=0} D_0 + \hat{\alpha} q_2^1 \Phi^{\hat{\theta}}_{k=1} D_1 \Big(\hat{\alpha} \Upsilon^{\hat{\theta}}_{k=0} D_0 + (1-\hat{\alpha}) I \Big) + (1-\hat{\alpha}) I \Big],
\end{aligned}$$

where D_k represents the Jacobian of the route cost functions evaluated at predicted flow $\boldsymbol{\pi}^{k,(t+1)}$ and Υ^{θ}_{k} the Jacobian of Logit operator with θ evaluated at $\boldsymbol{c}\Big(\boldsymbol{\pi}^{k,(t+1)}\Big)$.

Proof. The derivation can be found in Appendix G. □

6.2.2 Stability near the SUE

If $\theta \neq \hat{\theta}$, the block submatrices in (34) would not commute with each other, and thus $|\lambda I - J\Phi|$ entails directly calculating the inverse matrix of either one of these submatrices. However, none of these inverse submatrices has a closed-form. Hence, we analytically examine the case of $\theta = \hat{\theta}$ only.

Proposition 7. *Denote ρ_i as the i-th eigenvalue of $\Upsilon^{\theta}\big[\boldsymbol{c}(\tilde{\boldsymbol{x}}^{\star})\big] D\big[\tilde{\boldsymbol{x}}^{\star}\big]$ at the SUE under Assumption 1 and $\rho_i \leq 0, \forall i$. Define function $\psi(\rho_i; \alpha, \hat{\alpha}, p^0, p^1, p^2) \equiv \alpha\hat{\alpha}^2 p^2 \frac{p^1}{p^0+p^1} \rho_i^3 + (\alpha\hat{\alpha} - \alpha\hat{\alpha}p^0 - \alpha\hat{\alpha}^2 p^2 \frac{p^1}{p^0+p^1}) \rho_i^2 + (\alpha\hat{\alpha}p^0 - \alpha\hat{\alpha} + \alpha)\rho_i + (1-\alpha)$ where $p^0 + p^1 + p^2 = 1$. When $\hat{\theta} = \theta$ and $|K| \leq 3$, the*

SUE is locally asymptotically stable when $-1 < \psi(\rho_i; \alpha, \hat{\alpha}, p^0, p^1, p^2) < 1, \forall i$. *If* $|K| = 2$, *then* $p^2 = 0$. *If* $|K| = 1$, *then* $p^1 = p^2 = 0$, $p^0 = 1$ *and* $\hat{\alpha} = \alpha$.

Proof. See Appendix H. □

Remark 4. *Recall that the stability of the CH-NTP dynamic does not depend on the distribution of strategic thinking levels (i.e.,* p^0, p^1, *and* p^2*) when the projection operator always yields positive flows (see Proposition 3). In contrast, the proportions would affect the stability of the CH-Logit dynamic even though the Logit operator always generates positive flows.*

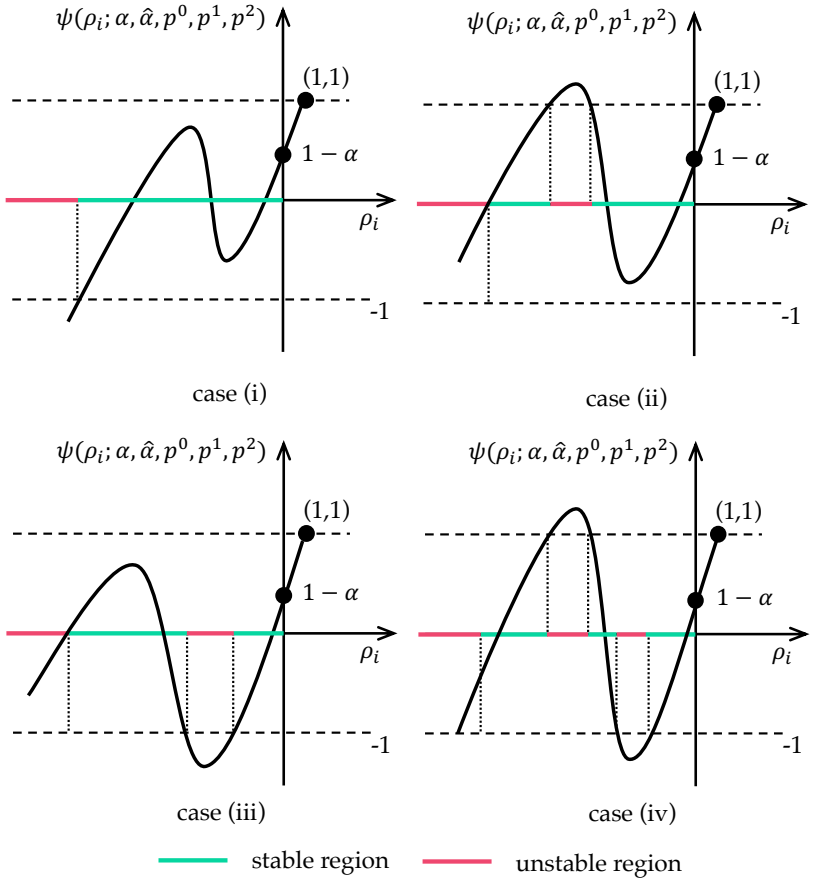

Figure 10: Sketches of stable and unstable regions of the CH-Logit dynamic under four possible scenarios of $\psi(\rho_i; \alpha, \hat{\alpha}, p^0, p^1, p^2)$.

Scrutinization of the cubic function $\psi(\rho_i; \alpha, \hat{\alpha}, p^0, p^1, p^2)$ shows that it crosses points $(1, 1)$ and $(0, 1-\alpha)$ and exhibits different shapes depending on $\alpha, \hat{\alpha}, p^0, p^1$ and p^2. Figure 10 depicts four possible scenarios when determining the stable region. Here the stable/unstable region refers to the region of the five parameters that make the SUE stable/unstable (i.e., whether or not $\psi(\rho_i; \alpha, \hat{\alpha}, p^0, p^1, p^2) \in (-1, 1), \forall \rho_i$). They are classified based on whether the cubic function has one or three real roots (which may not be distinct) at 1 or -1. The analytical results of the

stable region for $|K| = 3$ with $\hat{\alpha} \neq \alpha$ are quite cumbersome and do not reveal any direct insights. (They are thus omitted for simplicity.) Therefore, similar to the case of the CH-NTP dynamic, we turn to analyze two special cases below.

6.2.2.1 Perfect prediction

Even under $\hat{\alpha} = \alpha$, the stability condition of the CH-Logit dynamic given by Proposition 7 is much more complex than the CH-NTP dynamic. We explore the stability numerically. Given an eigenvalue ρ_i, we enumerate all the possible combinations of p^0 and p^1 in a resolution of 0.001 (p^2 is not required as $p^2 = 1 - p^0 - p^1$) with $\alpha \in \{0.2, 0.5, 0.8\}$ and check whether the stability condition is satisfied as per Proposition 7. Stable and unstable regions under different values of ρ_i are depicted in Figure 11. Some observations can be made on these plots:

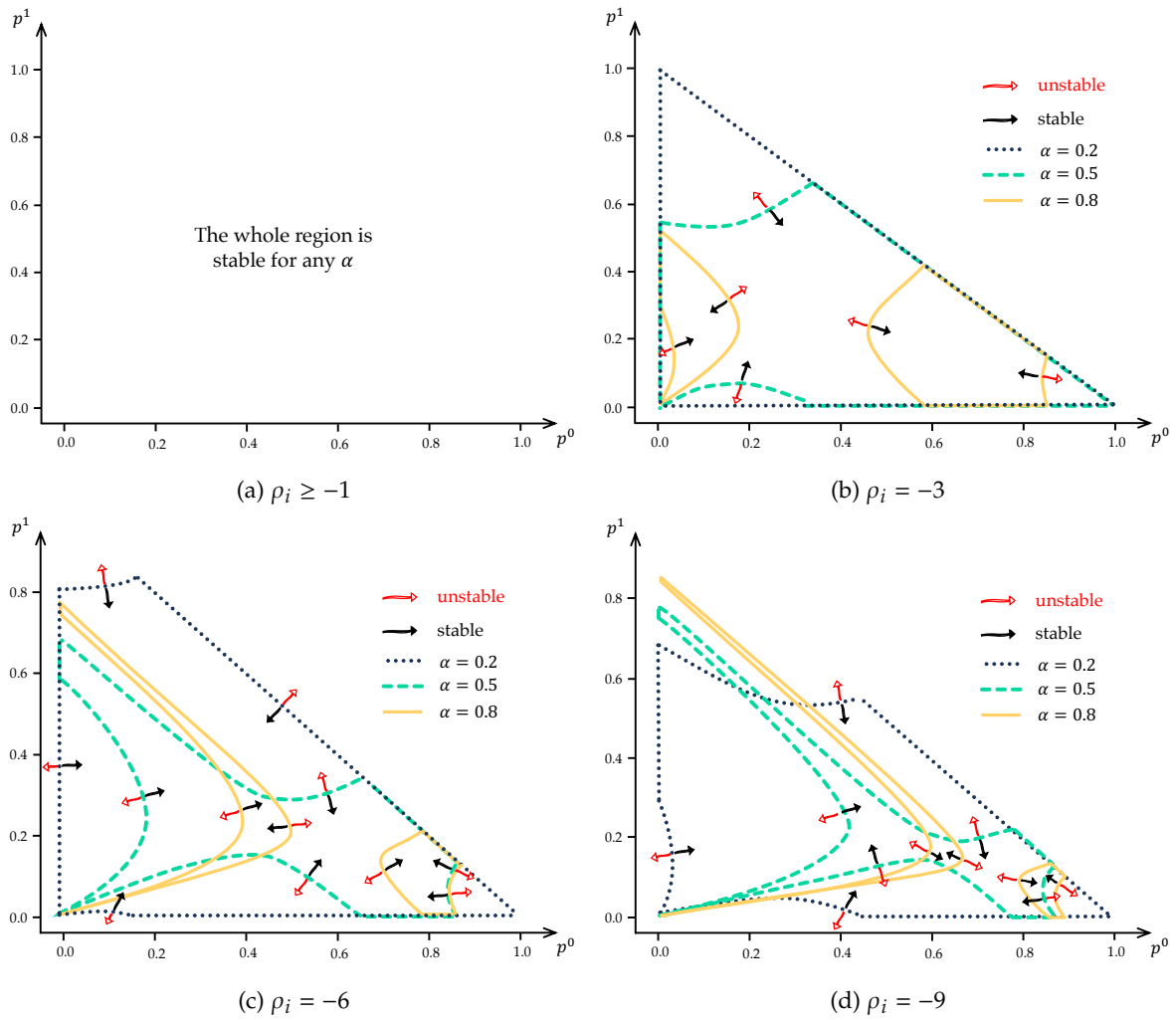

(a) $\rho_i \geq -1$ (b) $\rho_i = -3$

(c) $\rho_i = -6$ (d) $\rho_i = -9$

Figure 11: Stable and unstable regions of the CH-Logit dynamic with $\hat{\alpha} = \alpha$ w.r.t. different eigenvalues ρ_i.

(i) When $\rho_i \geq -1$, the system is always stable irrespective of any parameter. To explain, note

that $\psi(\rho_i = -1; \alpha, \hat{\alpha} = \alpha, p^0, p^1, p^2) = 2\alpha^2 - 2(p^0+1)\alpha + 1 = (\sqrt{2}\alpha - \frac{\sqrt{2}}{2}(1+p^0))^2 - \frac{1}{2}(1+p^0)^2 + 1$, which is greater than -1 because $p^0 \leq 1$ and $\alpha < 1$. Further note that when $\rho_i \in [-1, 0]$, the function monotonically increases in ρ_i. Hence, if $\rho_i \geq -1$, the cubic function is always greater than -1 but less than $1 - \alpha$;

(ii) Given a ρ_i in $(-\infty, -1)$, the stable region would gradually shrink as α increases. Moreover, the stable region would be separated into two pieces when α exceeds a certain threshold (approximately 0.6);

(iii) For a fixed small α that does not separate the stable region, a balanced pattern of p^0, p^1, and p^2 is more likely to be stable. In other words, an extremely small or large p^0, p^1, or p^2 would compromise the stability;

(iv) For a fixed large α that separates the stable region, as ρ_i decreases in $(-\infty, -1)$, the two pieces of stable regions tend to move rightward. It indicates that when the stability condition is restricted, a large p^0 is more likely to stabilize the system.

6.2.2.2 Imperfect prediction when $|K| = 2$

The cubic function $\psi(\rho_i; \alpha, \hat{\alpha}, p^0, p^1, p^2)$ in Proposition 7 reduces to a quadratic or linear function when $|K| = 2$ or 1, respectively. In these two cases, the stable region in terms of ρ_i can be succinctly described by the key parameters. Proposition 8 gives the results, followed by the discussions on how over- and under-predictions will affect the stability.

Proposition 8. *The CH-Logit dynamic with $|K| = 1$ is locally asymptotically stable at the SUE under Assumption 1 when $\rho_i > \frac{\alpha-2}{\alpha}, \forall i$. When $\hat{\theta} = \theta$, for $|K| = 2$, the SUE under Assumption 1 is locally asymptotically stable when one of the following two conditions holds for all ρ_i: (i) $1-\alpha+\frac{\alpha(1-\hat{\alpha}+\hat{\alpha}p^0)^2}{4\hat{\alpha}(p^0-1)} > -1$ and $\rho_i > \frac{1}{(p^0-1)\hat{\alpha}}$; or (ii) $1 - \alpha + \frac{\alpha(1-\hat{\alpha}+\hat{\alpha}p^0)^2}{4\hat{\alpha}(p^0-1)} < -1$ and $\{\rho_i : \frac{1}{(p-1)\hat{\alpha}} \leq \rho_i \leq f_0(\alpha, \alpha, p^0)\} \cup \{\rho_i : f_1(\alpha, \hat{\alpha}, p^0) \leq \rho_i < 0\}$. Here $f_0(\alpha, \hat{\alpha}, p^0) \equiv \frac{1}{2}(-\sqrt{\frac{\alpha(1+\hat{\alpha}-\hat{\alpha}p^0)^2+8\hat{\alpha}(p^0-1)}{\alpha\hat{\alpha}^2(p^0-1)^2}} + \frac{1}{\hat{\alpha}(p^0-1)} + 1)$, and $f_1(\alpha, \hat{\alpha}, p^0) \equiv \frac{1}{2}(\sqrt{\frac{\alpha(1+\hat{\alpha}-\hat{\alpha}p^0)^2+8\hat{\alpha}(p^0-1)}{\alpha\hat{\alpha}^2(p^0-1)^2}} + \frac{1}{\hat{\alpha}(p^0-1)} + 1)$.*

Proof. See Appendix I. □

Proposition 8 reveals insights into how the strategic-thinking behavior and associated over- and under-predictions affect the stability by comparing the stable region size between CH-Logit models with $|K| = 1$ and 2. The discussion is as follows.

Over-prediction ($\hat{\alpha} \geq \alpha$)

For case (i) of $|K| = 2$ in Proposition 8, solving $1 - \alpha + \frac{\alpha(1-\hat{\alpha}+\hat{\alpha}p^0)^2}{4\hat{\alpha}(p^0-1)} > -1$ with $\hat{\alpha} \geq \alpha$ yields $p^0 \leq h(\alpha, \hat{\alpha}) \equiv 2\sqrt{2}\sqrt{-\frac{\alpha-2}{\alpha^2\hat{\alpha}^2}} + \frac{\alpha\hat{\alpha}+\alpha-4}{\alpha\hat{\alpha}}$. Noting that $h(\alpha, \hat{\alpha})$ is monotonically increasing in $\hat{\alpha}$ and $h(\alpha, \hat{\alpha} = \alpha) \geq 2(\sqrt{2}-1)$, we obtain $h(\alpha, \hat{\alpha}) \geq 2(\sqrt{2}-1) \approx 0.828$. The stability condition for $|K| = 1$ requires all the $\rho_i > \frac{\alpha-2}{\alpha}$ while the condition for $|K| = 2$ needs all the $\rho_i > \frac{1}{(p^0-1)\hat{\alpha}}$. Comparing these two thresholds yields: $\frac{1}{(p^0-1)\hat{\alpha}} - \frac{\alpha-2}{\alpha} < 0$ when $p^0 > g(\alpha, \hat{\alpha}) \equiv \frac{\alpha\hat{\alpha}+\alpha-2\hat{\alpha}}{\alpha\hat{\alpha}-2\hat{\alpha}}$ and $\frac{1}{(p^0-1)\hat{\alpha}} - \frac{\alpha-2}{\alpha} > 0$ when $p^0 < g(\alpha, \hat{\alpha})$. Hence, the stable region is expanded when $g(\alpha, \hat{\alpha}) < p^0 < h(\alpha, \hat{\alpha})$, and shrunk when $0 < p^0 < g(\alpha, \hat{\alpha})$.

For case (ii) of $|K| = 2$, $p^0 > h(\alpha, \hat{\alpha})$. Combined size of the two separated stable regions over ρ_i is $f_0(\alpha, \hat{\alpha}, p^0) - \frac{1}{(p-1)\hat{\alpha}} + 0 - f_1(\alpha, \hat{\alpha}, p^0) = \frac{1}{\hat{\alpha}(1-p^0)} \cdot \left(1 - \sqrt{\frac{8\hat{\alpha}(p^0-1)+\alpha(1+\hat{\alpha}-p^0\hat{\alpha})^2}{\alpha}}\right)$, which is always less than $\frac{2-\alpha}{\alpha}$ when $p^0 > h(\alpha, \hat{\alpha})$. Hence, the total size of the two separated stable regions is expanded.

Figure 12 summarizes the above discussion by depicting how the stable region alters when $|K|$ changes from 1 to 2 under different p^0, α, $\hat{\alpha}$. Note how the parametric space of p^0 and α with a shrinking stable region enlarges as over-prediction becomes more severe (i.e., $\frac{\hat{\alpha}}{\alpha}$ becomes larger).

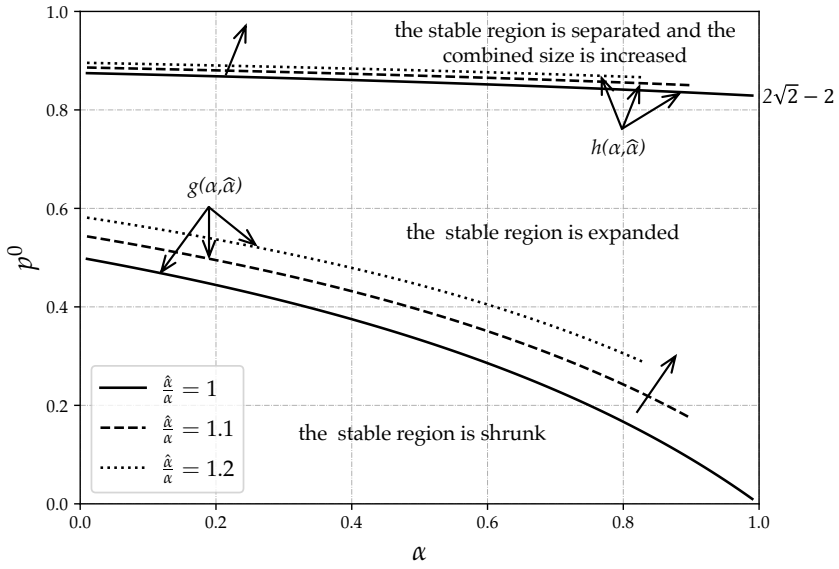

Figure 12: Sketch of how the stable region alters when $|K|$ changes from 1 to 2 under different p^0, α, $\hat{\alpha}$, and $\hat{\alpha} \geq \alpha$.

Under-prediction ($\hat{\alpha} \leq \alpha$)

Scenario (1): $\hat{\alpha} > 3 - 2\sqrt{2}$

Consider first case (i) of $|K| = 2$ in Proposition 8 where $f^*(\alpha, \hat{\alpha}, p^0) > -1$ and $p^0 < h(\alpha, \hat{\alpha})$. The discussion is divided into two sub-cases:

- when $\hat{\alpha} \geq \frac{\alpha}{2-\alpha}$, solving $\frac{1}{(p^0-1)\hat{\alpha}} < \frac{\alpha-2}{\alpha}$ yields $p^0 > g(\alpha, \hat{\alpha})$ and solving $\frac{1}{(p^0-1)\hat{\alpha}} > \frac{\alpha-2}{\alpha}$ obtains $p^0 < g(\alpha, \hat{\alpha})$. Hence, the region is expanded when $g(\alpha, \hat{\alpha}) < p^0 < h(\alpha, \hat{\alpha})$ and shrunk when $p^0 < g(\alpha, \hat{\alpha})$. It can be verified that $g(\alpha, \hat{\alpha})$ is monotonically increasing in $\hat{\alpha}$ and that $h(\alpha, \hat{\alpha}) - g(\alpha, \hat{\alpha})$ is monotonically decreasing in $\hat{\alpha}$ when $0 < \alpha, \hat{\alpha} < 1$. Hence, the parametric space of p^0, α, and $\hat{\alpha}$ ($< \alpha$) rendering the stable region shrunk is smaller than the perfect prediction case, while the parametric space leading to an expanded stable region is larger than the perfect prediction case;
- when $\hat{\alpha} < \frac{\alpha}{2-\alpha}$, $\frac{1}{(p^0-1)\hat{\alpha}} < \frac{\alpha-2}{\alpha}$ always holds and thus the expanded region is simply $p^0 < h(\alpha, \hat{\alpha})$. When prediction behaviors are considered, no stable region of $|K| = 1$ is shrunk.

For case (ii) where $f^*(\alpha, \hat{\alpha}, p^0) < -1, p^0 > h(\alpha, \hat{\alpha})$, it is verified that $f_0(\alpha, \hat{\alpha}, p^0) - \frac{1}{(p-1)\hat{\alpha}} + 0 - f_1(\alpha, \hat{\alpha}, p^0) > \frac{2-\alpha}{\alpha}$. Hence, when $p^0 > h(\alpha, \hat{\alpha})$, the stable region is separated and the combined stable region size increased. Since $h(\alpha, \hat{\alpha})$ is monotonically increasing in $\hat{\alpha}$, the parametric space rendering the total size of the stable region greater is larger than the perfect prediction case.

The above discussion is summarized in Figure 13. Note how the parametric space of p^0 and α with an expanding stable region enlarges as a "moderately" small $\hat{\alpha} \in (3 - 2\sqrt{2}, \alpha)$ increases. In other words, a mild under-prediction helps stabilize the CH-Logit dynamic, which is very similar to the finding of the CH-NTP dynamic.

Scenario (2): $\hat{\alpha} < 3 - 2\sqrt{2}$

This scenario depends on the comparison between $\frac{8\hat{\alpha}}{(1+\hat{\alpha})^2}$ and α. When $\frac{8\hat{\alpha}}{(1+\hat{\alpha})^2} > \alpha$, discussion is the same as the case of $\hat{\alpha} > 3 - 2\sqrt{2}$; i.e., it helps stabilize the dynamic. When $\frac{8\hat{\alpha}}{(1+\hat{\alpha})^2} < \alpha$, $f^*(\alpha, \hat{\alpha}, p^0) < -1$ always holds and thus the stable region is separated, while the combined size is increased. The latter case is similar to the CH-NTP dynamic with $\hat{\gamma} < \frac{\gamma}{2}$.

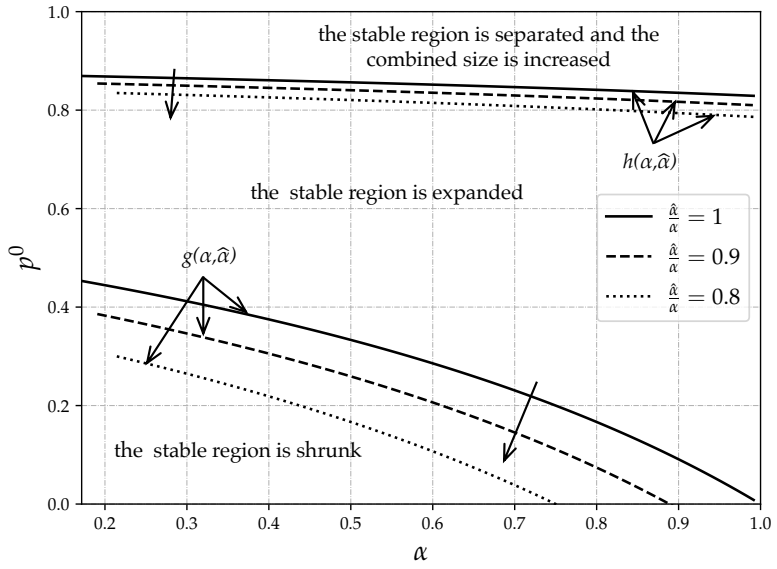

Figure 13: Sketch of how the stable region changes when $|K|$ changes from 1 to 2 under different p^0, α, $\hat{\alpha}$ and $3-2\sqrt{2}<\hat{\alpha}\leq\alpha$.

Summary

The CH-Logit dynamic bears similarity to the CH-NTP dynamic on how under- and over-predictions affect the stability near the UE. Over-predictions ($\hat{\alpha}>\alpha$ for CH-Logit dynamic and $\hat{\gamma}>\gamma$ for CH-NTP dynamic) render the system less stable while mild under-predictions ($3-2\sqrt{2}<\hat{\alpha}<\hat{\alpha}$ for CH-Logit dynamic and $\frac{\gamma}{2}<\hat{\gamma}<\gamma$ for CH-NTP dynamic) help stabilize the small perturbations near the UE. Severe under-predictions ($\hat{\alpha}<3-2\sqrt{2}$ and $\frac{8\hat{\alpha}}{(\hat{\alpha}+1)^2}<\alpha$ for CH-Logit dynamic and $\hat{\gamma}<\frac{\gamma}{2}$ for CH-NTP dynamic) separate the stable region into two pieces while the total size of the region is increased.

When more travelers tend to strategically predict others' behaviors (i.e., a larger p^1), the system becomes less stable and behaves like the over-prediction case.

Numerical experiments pertaining to the CH-Logit dynamic confirm the above theoretical results. They are omitted here for simplicity since the results and findings (such as the multi-equilibria phenomenon) are similar to the case of the CH-NTP dynamic, except that the DUE becomes the SUE.

7 Conclusions and Future Research

This paper developed a new modeling framework of day-to-day network flow dynamics that incorporates hierarchical cognitive levels (Camerer et al., 2004) to better capture travelers'

dynamic re-routing behaviors. The classical NTP and Logit dynamics, on behalf of the DUE and SUE cases, respectively, were extended into the framework. Considering heterogeneity in travelers' strategic-reasoning levels, the proposed CH-NTP model significantly improved the goodness-of-fit for a recent virtual experiment, which traditional day-to-day models could not achieve. For both dynamics, stationary states and local stabilities near the user equilibria were theoretically analyzed and verified by numerical experiments.

We find that in addition to converging to the classical user equilibria (DUE/SUE), the proposed dynamics may also converge to other equilibria, depending on the initial conditions and parameters. For example, with a large γ, different initial conditions lead to different equilibria, while under a small γ, various initial points tend to evolve to the same DUE tardily (see again Figures 5a and b). Moreover, when higher-step travelers can accurately predict lower-step ones' switching propensities, thinking multiple steps ahead does not affect the local stability of the CH-NTP dynamic around the DUE, and the stability condition does not depend on the distribution of strategic-reasoning levels. In comparison, the stability condition for the CH-Logit dynamic largely depends on the proportion of heterogeneous travelers. Finally, we find that for both dynamics with $|K| = 2$: (i) when 1-step travelers over-predict 0-step ones' switching propensity, the stable region is shrunk, and when the over-prediction is severe (e.g., $\hat{\gamma} > \bar{\gamma}$ for the CH-NTP dynamic), the UE is always unstable; (ii) when 1-step travelers *moderately* under-predict 0-step ones' re-routing tendency, the stable region is increased; and (iii) when the under-predictions are severe, the stable region is separated into two parts.

Despite the fresh findings generated, our models still have limitations, which may direct future research. First, we select two widely-used day-to-day models from the literature as examples of the general modeling framework. Many more classical day-to-day models can be analyzed in the future (e.g., Smith, 1979b, 1983; Nagurney and Zhang, 1997; Jin, 2007; Xiao et al., 2019), including those that consider travelers' learning behavior (Horowitz, 1984; Cantarella and Cascetta, 1995; Bie and Lo, 2010). We surmise that findings on local stability still generally hold when hierarchical cognitive behaviors are incorporated into these models, provided that the dynamic itself exhibits similar properties (e.g., negative definiteness of the Jacobian). Second, the virtual experiment data suggest that travelers' re-routing tendencies become weaker through repeated game play. Further research can use time-varying parameters to capture such a phenomenon better. Third, future research can investigate how different measures, such as congestion tolling (Tan et al., 2015; Guo et al., 2016; Liu et al., 2017; Han

et al., 2017), traffic control (Smith, 1979a; Köhler and Strehler, 2019), and information provision schemes (Liu and Szeto, 2020), can improve the system performance. Due to the multi-equilibria phenomenon, it would be interesting to drive the traffic system to the desired state via these measures. Han et al. (2017) showed the possibility of using congestion tolling to direct traffic evolution to the target stationary state from any initial states when multiple equilibria exist. Our current research efforts are aimed in this direction.

Acknowledgement

The research was supported by the National Natural Science Foundation of China (Project No.'s 72201214 and 72025104) and the Sichuan Science and Technology Program (Project No. 2023NSFSC1035).

Appendix A Definitions and theorems on local stability and block matrices

Definition A.1. *Suppose $\boldsymbol{x}^{\dagger}$ is an equilibrium point (fixed point) of the discrete autonomous system:*

$$\boldsymbol{x}^{(t+1)} = \phi(\boldsymbol{x}^{(t)}). \tag{A.1}$$

$\boldsymbol{x}^{\dagger}$ is said to be:

(i) locally stable if given any $\epsilon > 0$, there exists a $\delta(\epsilon) > 0$ such that

$$||\boldsymbol{x}^{(0)} - \boldsymbol{x}^{\dagger}|| < \delta(\epsilon) \rightarrow ||\boldsymbol{x}^{(t)} - \boldsymbol{x}^{\dagger}|| < \epsilon, \forall t = 1, 2, 3, \ldots; \tag{A.2}$$

(ii) locally asymptotically stable if there exists an $\eta > 0$ such that:

$$||\boldsymbol{x}^{(0)} - \boldsymbol{x}^{\dagger}|| < \eta \rightarrow \lim_{t \rightarrow \infty}(\boldsymbol{x}^{(t)}) = \boldsymbol{x}^{\dagger}; \tag{A.3}$$

and

(iii) unstable if (i) is not true.